New Quantum Cascade Laser Architectures

II–VI Quantum Cascade Emitters, High k-Space Lasing, & Short Injectors

Kale J. Franz

A Dissertation
Presented to the Faculty
of Princeton University
in Candidacy for the Degree
of Doctor of Philosophy

Recommended for Acceptance
by the Department of Electrical Engineering

Adviser: Claire Gmachl

June 2009

Chapter 2

Quantum Cascade Laser Design and Operation Theory

Because of the inherent flexibility afforded by the QC concept, laser designs are highly customizable. And to optimize a design for any particular goal or set of operating conditions, a basic understanding of the contributions of various laser parameters to performance is key.

In this chapter, I provide the basic tools and derive the fundamental relations important to QC laser design and operation. In sum, it is a QC laser "toolbox" generally applicable to most QC laser design circumstances. Individually, the foundations for most sections of this chapter can be found in the references cited herein. However, no single reference exists that thoroughly covers all the aspects important to QC laser design. This chapter thus compiles knowledge garnered from a number of disparate sources. Furthermore, where I have found no good source for elements I believe to be crucial to QC laser design, I provide a thorough, original discussion.

This theory becomes the foundation for ideas presented in later chapters, and it also provides a basis for new insights and understanding derived from the data presented in the remainder of this thesis.

2.1 The Schrödinger Equation

Fundamental to QC laser design is the ability to accurately calculate the positions of energy states in the quantum-confined dimension. Generally, we are most interested in

the conduction band wavefunctions ψ_{C}. In the elementary abstraction, we simply solve the time-independent Schrödinger equation

$$-\frac{\hbar^2}{2m^*}\frac{\partial^2}{\partial z^2}\psi_{\mathrm{C}}(z)+qV_{\mathrm{C}}(z)\psi_{\mathrm{C}}(z)=\mathcal{E}_q\psi_{\mathrm{C}}(z) \tag{2.1}$$

where $\hbar$ is Planck's constant, m^* is the conduction band effective mass, z is the dimension of quantum confinement, qV_{C} is the conduction band potential energy profile, and $\mathcal{E}_q$ is the eigen energy of the quantum state.

Immediately, we encounter a problem. Coupling of the conduction band energy states with the valence bands and other bands makes the solution much more complex than the simple one-band model of Eq. (2.1). However, for our primary interest of bound conduction band solutions, these complex interactions can be reduced to an energy-dependence of the effective conduction band mass [27]. Consequently, as the electron acquires more energy—*i.e.* gets higher up in the band and closer to the vacuum level—the electron gets "heavier." Also, our QC structure is a system of layered materials, each with a different effective mass from adjacent layers. So, the effective mass is both energy- and position-dependent: $m^*(z,\mathcal{E})$. This results in a small change to the simple Schrödinger equation. When solving the Schrödinger equation, we are taught to match $\psi_{\mathrm{C}}(z)$ and $\frac{\partial}{\partial_z}\psi_{\mathrm{C}}(z)$ at the boundaries. Now, with variable effective masses, the solutions of envelope functions [28] are continuous across material interfaces in both $\psi_{\mathrm{C}}(z)$ and $\frac{1}{m^*}\frac{\partial}{\partial z}\psi_{\mathrm{C}}(z)$.

Because of variable effective mass, the classical portrayal of the Schrodinger equation is somewhat different. Given the momentum operator $\mathcal{P}_z=-\mathrm{i}\hbar\partial_{\mathrm{z}}$, the kinetic energy operator $\mathcal{T}$ becomes [27]

$$\mathcal{T}=\mathcal{P}_z\frac{1}{2m^*(z,\mathcal{E})}\mathcal{P}_z=-\frac{\hbar^2}{2}\frac{\partial}{\partial z}\frac{1}{m^*(z,\mathcal{E})}\frac{\partial}{\partial z} \tag{2.2}$$

and the Schrödinger equation now becomes

$$-\frac{\hbar^2}{2}\frac{\partial}{\partial z}\frac{1}{m^*(z,\mathcal{E})}\frac{\partial}{\partial z}\psi_{\mathrm{C}}(z)+qV_{\mathrm{C}}(z)\psi_{\mathrm{C}}(z)=\mathcal{E}_q(z)\psi_{\mathrm{C}}(z) \tag{2.3}$$

where $\mathcal{E}_q(z)$ acquires a position-dependence when defined as the energy relative to the conduction band edge and in the presence of an applied electric field E_{field}. Now, to

make Eq. (2.3) discrete, we approximate the derivative as

$$\frac{df}{dz} \approx \frac{\Delta f}{\Delta z} = \frac{f(z+\delta z) - f(z-\delta z)}{2\delta z} . \tag{2.4}$$

The Schrödinger equation above can be discretized by expanding $\mathcal{T}\psi_c(z)$.

$$\frac{\frac{1}{m^*(z+\delta z,\mathcal{E})}\frac{\partial\psi(z)}{\partial z}\Big|_{z+\delta z} - \frac{1}{m^*(z-\delta z,\mathcal{E})}\frac{\partial\psi(z)}{\partial z}\Big|_{z-\delta z}}{2\delta z} = \frac{2}{\hbar^2}[qV_c(z) - \mathcal{E}]\psi_c(z) \tag{2.5}$$

Applying Eq. (2.4) to the above equation, gathering terms in $\psi_c(z)$, and making the transformation $2\delta z \rightarrow \delta z$ gives

$$\begin{aligned}\psi_c(z+\delta z) = \Bigg\{\left[\frac{2(\delta z)^2}{\hbar^2}[qV(z)_c - \mathcal{E}] + \frac{1}{m^*(z+\delta z/2,\mathcal{E})} + \frac{1}{m^*(z-\delta z/2,\mathcal{E})}\right]\psi(z) \\ - \frac{1}{m^*(z-\delta z/2,\mathcal{E})}\psi(z-\delta z)\Bigg\} m^*(z+\delta z/2,\mathcal{E})\end{aligned} \tag{2.6}$$

The effective mass at the intermediate points $z \pm \delta z/2$ is found by taking the average of the effective mass for the two adjacent points z and $z+\delta z$. By virtue of having coupled quantum well structures with abrupt material interfaces and the presence of varying electric fields, all parameters related to wavefunctions, energies, effective masses, etc. will be implicitly assumed to have position-dependence z, and these references will be hereafter dropped when not explicitly needed.

The shooting method is used to solve for the eigen energies of our system through the application of Eq. (2.6). Specifically, we look for bound solutions of the system confined by the dimensions $z = 0$ and $z = z_{end}$. That is, any energy $\mathcal{E}$ where $\psi(0) = 0$ and $\psi(z_{end}) = 0$. In an elementary implementation of the shooting method, the energy space covered by our potential $V_c(z)$ is initially divided into many discrete steps. Then, Eq. (2.6) is used to propagate through discrete steps in z to find $\psi(z_{end})$ for each initial energy value, where the initial conditions $\psi(0) = 0$ and $\psi(z_{second}) = 1$ are used (z_{second} being the second discrete solve point after $z = 0$). To find the exact energy value of a bound solution, we take advantage of the fact that $\psi(z_{end})$ switches signs at a bound solution. Therefore, when $\psi(z_{end})$ is plotted for all energies over our energy space, noting the location in energy of a sign flip of $\psi(z_{end})$, allows us to iterate in energy around this point

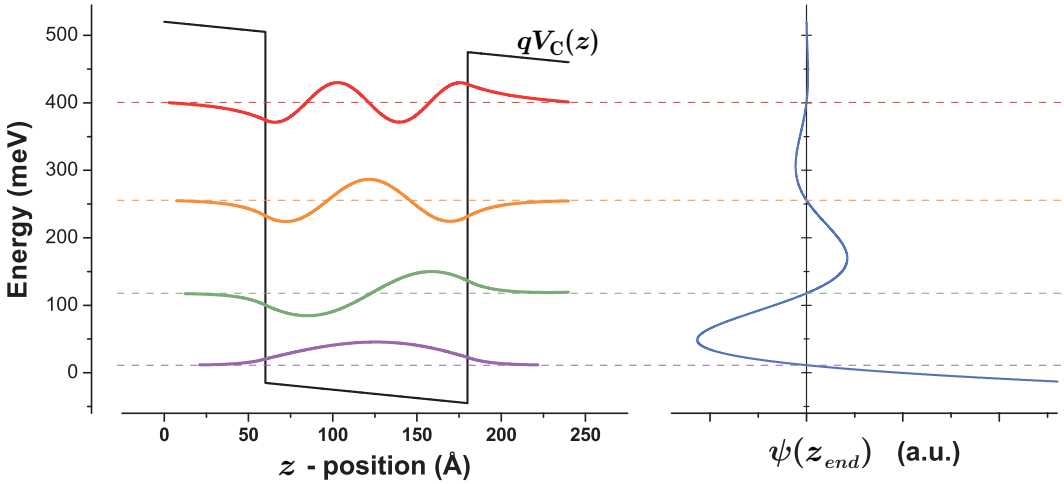

Figure 2.1: Example use of the shooting method. The left panel shows a potential $V(z)$ for an $In_{0.53}Ga_{0.47}As$ / $Al_{0.48}In_{0.52}As$ quantum well with $E_{field} = 25$ kV/cm. Four bound solutions are found by finding the roots of $\psi(z_{end})$, as shown in the right panel. The wavefunction $\psi(z)$ is plotted for the four bound solutions.

to find the exact value of the bound solution. Figure 2.1 provides an example; here, our potential $V_c(z)$ is for a single quantum well in the $In_{0.53}Ga_{0.47}As$ / $Al_{0.48}In_{0.52}As$ system, with conduction band offset of 520 meV, and an applied electric field $E_{field} = 25$ kV/cm. Four bound solutions are found, and $\psi_t nC(z)$ is plotted for each solution, using the eigen energy as the baseline of the wavefunction.

2.2 Interface Energy Offsets and Bandgaps

To properly use Eq. (2.6) for solving the time-independent Schrödinger equation, we need accurate knowledge of two key parameters: $V_c(z)$ and $m^*(z,\mathcal{E})$. This section is devoted to attaining the band offset values that are so important to coupled quantum well systems such as QC lasers. In the following section, we discuss effective mass in semiconductor systems. This section and the remaining sections in this chapter make heavy use of semiconductor materials parameters; a superb review of important III–V material parameters was published by Vurgaftman *et al.* in 2001 [29], and is summarized in Tables 2.1 and 2.2 for common III–V QC materials.

All QC laser implementations to date have used intersubband transitions in the conduction band. While QC electroluminescence has been shown from valence intersubband transitions [30] [31], we are more keenly interested in the conduction band edge offsets of materials. As it turns out, the valence band offsets have been much more extensively studied [29], owing to the experimental difficulty of measuring conduction band offsets. When considering a valence band offset, the convention is to report the parameter VBO, which is the valence band offset relative to a predetermined reference material where VBO is specified as 0 (*i.e.* $VBO = 0$); Vurgaftman *et al.*, for example, define $VBO(\text{InSb}) = 0$. In this way, the valence band offset for any two arbitrary materials is easily found as the difference in VBO for the two materials of the set. By adding the bandgap of each material to its respective VBO, the conduction band offset for a two material system can likewise be calculated. More concretely, the conduction band edge (at the Γ point) $\mathcal{E}_c^\Gamma$ can be defined as

$$\mathcal{E}_c^\Gamma = VBO + \mathcal{E}_g^\Gamma + \delta\mathcal{E}_{Varsh} + \delta\mathcal{E}_{\varepsilon c} + \delta\mathcal{E}_{\varepsilon v} \tag{2.7}$$

where $\mathcal{E}_g^\Gamma$ is the energy gap at the Γ point at temperature $T = 0$ K without strain, $\delta\mathcal{E}_{Varsh}$ is the Varshney correction to the bandgap energy for $T \neq 0$ K, and $\delta\mathcal{E}_{\varepsilon c}$ and $\delta\mathcal{E}_{\varepsilon v}$ are corrections to the conduction and valence band edges due to hydrostatic deformation (*i.e.* strain). Each of these terms is treated in the following sections. With this definition of $\mathcal{E}_c^\Gamma$, the conduction band offset at the interface between two materials A and B is $\Delta\mathcal{E}_c^\Gamma = \mathcal{E}_c^\Gamma(A) - \mathcal{E}_c^\Gamma(B)$.

2.2.1 Materials parameters for ternary alloys

Fundamental materials parameters, VBO and $\mathcal{E}_g^\Gamma$ for example, can be conveniently reported in tabular form for binary semiconductors, as in the review by Vurgaftman *et al.* [29]. Ternary alloys, however, have a degree of freedom in material composition, making tabular recording prohibitive. For any ternary material $A_xB_{1-x}C$, composed proportionally of the two constituent binaries $(AC)_x$ and $(BC)_{1-x}$, a range of values exists over the mole fraction x for any generic material parameter P. Conveniently, we can make use of the composition endpoints $x = 0$ and $x = 1$ to bound the possible values

Table 2.1: Material parameters for the binary alloys InAs, GaAs, and AlAs. Source is [29], unless otherwise indicated. Lattice constants are given for 300 K. The effective mass is given for the bulk band edge, with m_0 the free electron mass.

	InAs	GaAs	AlAs
$a_{\ell c}$ (Å)	6.0583	5.6533	5.6611
c_{11} (GPa)	832.9	1221	1250
c_{12} (GPa)	452.6	566	534
$\mathcal{E}_G^\Gamma$ (eV)	0.417	1.519	3.099
Δ_{SO} (eV)	0.39	0.341	0.28
VBO (eV)	-0.59	-0.80	-1.33
a_c^Γ (eV)	-5.08	-7.17	-5.64
a_v (eV)	-1.00	-1.16	-2.47
b (eV)	-1.8	-2.0	-2.3
$\mathcal{E}_P$ (eV)	21.5	28.8	21.1
F	-2.90	-1.94	-0.48
m_e^Γ / m_0	0.026	0.067	0.15
α^Γ (meV/K)	0.276	0.5405	0.885
β^Γ (K)	93	204	530
ϵ_s	14.3[1]	12.90[1]	10.06[1]
ϵ_∞	11.6[1]	10.86[1]	8.16[1]
$\hbar\omega_{LO}$	29.93[1]	35.3[1]	49.8[1]

(1) Ref. [32]

of P. Then, P can thus be defined as

$$P(A_xB_{1-x}C) = xP(AC) + (1-x)P(BC) + x(1-x)C_B \tag{2.8}$$

where C_B is the bowing parameter specific to material ABC. Commonly, the bowing parameter is either not well known, or no bowing parameter exists. In the case of $C_B = 0$, the material parameter is just a linear interpolation between the value of the parameter for the two component binaries weighted by x. Bowing parameters common for III–V QC materials are given in Table 2.2.

Table 2.2: Non-zero bowing parameters C_B for the ternary alloys InGaAs and AlInAs. Source is [29].

	InGaAs	AlInAs
$\mathcal{E}_G^\Gamma$ (eV)	0.477	0.70
Δ_{SO} (eV)	0.15	0.15
VBO (eV)	-0.38	-0.64
$\mathcal{E}_P$ (eV)	-1.48	-4.81
F	1.77	-4.44
m_e^Γ/m_0	0.0091	0.049
a_c^Γ (eV)	2.61	-1.4

2.2.2 Temperature effects on bandgap

The temperature dependence of semiconductor bandgaps is commonly described with the Varshni formula. This is an empirical formula that fits two Varshni parameters—α [$\frac{\text{energy}}{\text{temperature}}$] and β [temperature]—to experimentally obtained values of bandgap with temperature. The Varshni formula gives the temperature T dependence of the bandgap as [33]

$$\mathcal{E}_g(T) = \mathcal{E}_g(T=0) - \frac{\alpha T^2}{T+\beta} \tag{2.9}$$

so that the temperature correction to the conduction band edge is

$$\delta\mathcal{E}_{Varsh} = -\frac{\alpha T^2}{T+\beta}\,. \tag{2.10}$$

The Varshney corrections for the common QC materials $In_{0.53}Ga_{0.47}As$ and $Al_{0.48}In_{0.52}As$ are plotted in Fig. 2.2.

2.2.3 Strain effects on bandgap and band offset

Strain in epitaxially-grown semiconductors arises when the lattice constant for a particular composition of grown material is different from that of the substrate material. Generally, strain is an undesired condition, as strain buildup will eventually lead to a variety of epitaxial defects. The lattice constant and bandgap are both functions of the

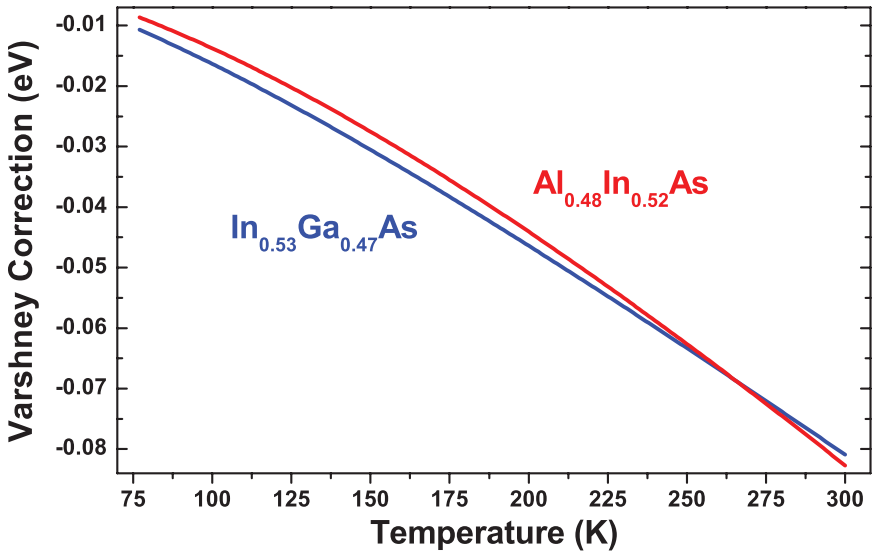

Figure 2.2: Bandgap temperature dependence. The Varshney correction $\delta\mathcal{E}_{Varsh}$ is plotted for the InP-lattice-matched compositions $In_{0.53}Ga_{0.47}As$ and $Al_{0.48}In_{0.52}As$. The effect of increasing temperature is the lowering of the material bandgap.

mole fraction x for any particular ternary material composition; therefore, imposing the condition that all grown materials are lattice-matched to the substrate lattice constant does not generally allow one to adjust mole fraction compositions to alter the material bandgap.*

Since QC lasers operate on intersubband transitions, any optical transition must be confined within the quantum wells of the heterostructure to prevent electrons from escaping. It is thus easy to see that the ability to adjust material compositions to maximize the conduction band offset would be advantageous. This is especially true when seeking high energy, short wavelength photon generation.

The QC concept allows for a clever way to achieve both strain-free bulk material while simultaneously having the ability to adjust material compositions to affect bandgaps. Taking advantage of the alternating layer structure, where a wide bandgap barrier material is interleaved with a narrow bandgap well material, compressive strain can be built into one layer set while tensile strain is built into the other layer set; the result can be an overall strain-balanced heterostructure [34].

* The materials systems GaAs/AlAs and InAs/AlSb represent a special exception where the binary pairs share a nearly identical lattice constant.

Semiconductors with a zinc blende lattice structure (cubic symmetry)—the case for most III–V alloys—acquire biaxial strain when epitaxially grown on a substrate with a different lattice constant. That means, for the three dimensional strain tensor, only the diagonal components ε_{xx}, ε_{yy}, and ε_{zz} are non-zero. Identifying z as the direction of epitaxial growth, values for strain are given by [35]

$$\varepsilon_{xx} = \varepsilon_{yy} = \frac{a_0 - a_{\ell c}}{a_{\ell c}} \tag{2.11a}$$

$$\varepsilon_{zz} = -\frac{2c_{12}}{c_{11}}\varepsilon_{xx} \tag{2.11b}$$

where a_0 is the lattice constant of the substrate, $a_{\ell c}$ is the lattice constant of the epitaxial layer material, and c_{11} and c_{12} are the elastic stiffness constants of the layer material.

The effects of strain on bandgaps are well described by the Pikus–Bir interaction [36] and also by the "model-solid" theory of Van de Walle [37]. Here, the change in band gap due to strain is empirically characterized by the relative change in volume $\mathcal{V}$ due to strain and scaled by a hydrostatic deformation potential a [energy] for both bands. The percent change in volume due to strain is given by

$$\frac{\delta\mathcal{V}}{\mathcal{V}} = \varepsilon_{xx} + \varepsilon_{yy} + \varepsilon_{zz} \tag{2.12}$$

which is the trace of the strain tensor. The change in bandgap due to strain $\delta\mathcal{E}_\varepsilon$ is then

$$\delta\mathcal{E}_\varepsilon = a\frac{\delta\mathcal{V}}{\mathcal{V}} \tag{2.13}$$

and the components of the shift acquired by the conduction and valence bands, $\delta\mathcal{E}_{\varepsilon c}$ and $\delta\mathcal{E}_{\varepsilon v}$ respectively, are

$$\delta\mathcal{E}_{\varepsilon c} = a_c\frac{\delta\mathcal{V}}{\mathcal{V}} \tag{2.14a}$$

$$\delta\mathcal{E}_{\varepsilon v} = a_v\frac{\delta\mathcal{V}}{\mathcal{V}} \tag{2.14b}$$

where a_c and a_v are the conduction and valence band hydrostatic deformation potentials, given that $a = a_c + a_v$. In compound semiconductors, adding hydrostatic pressure (*i.e.* adding compressive strain) results in an increase in band gap. Generally, this means

that compressive strain causes the conduction band edge to move "up" proportionally by $\frac{a_c}{a}$ and the valence band edge to move "down" proportionally by $\frac{a_v}{a}$.

The light hole (LH), heavy hole (HH), and split-off (SO) valence bands have p-state "shape" and therefore lack spherical symmetry, unlike the conduction band (C) with s-state shape. Due to this lack of symmetry, biaxial strain has a shear component that affects the valence bands, and it splits the degeneracy of the heavy hole and light hole bands at the Γ point. Derived from the Pikus–Bir Hamiltonian [36], the energy bandgaps with shear strain and including the spin-orbit interaction are

$$\mathcal{E}^{\Gamma}_{\mathrm{C-HH}} = \mathcal{E}^{\Gamma}_{g} + \delta\mathcal{E}_{\varepsilon c} + \delta\mathcal{E}_{\varepsilon v} - Q_{\varepsilon} \tag{2.15a}$$

$$\mathcal{E}^{\Gamma}_{\mathrm{C-LH}} = \mathcal{E}^{\Gamma}_{g} + \delta\mathcal{E}_{\varepsilon c} + \delta\mathcal{E}_{\varepsilon v} + \frac{1}{2}\left(Q_{\varepsilon} - \Delta_{\mathrm{SO}} + \sqrt{\Delta^2_{\mathrm{SO}} + 2\Delta_{\mathrm{SO}}Q_{\varepsilon} + 9Q^2_{\varepsilon}}\right) \tag{2.15b}$$

$$\mathcal{E}^{\Gamma}_{\mathrm{C-SO}} = \mathcal{E}^{\Gamma}_{g} + \delta\mathcal{E}_{\varepsilon c} + \delta\mathcal{E}_{\varepsilon v} + \frac{1}{2}\left(Q_{\varepsilon} - \Delta_{\mathrm{SO}} - \sqrt{\Delta^2_{\mathrm{SO}} + 2\Delta_{\mathrm{SO}}Q_{\varepsilon} + 9Q^2_{\varepsilon}}\right) \tag{2.15c}$$

where Δ_{SO} is the split-off energy without strain and the shear deformation potential b [energy] is included in Q_{ε}, defined as

$$Q_{\varepsilon} = \frac{b}{2}\left(\varepsilon_{xx} + \varepsilon_{yy} - 2\varepsilon_{zz}\right) . \tag{2.16}$$

The bandgaps given in Eq. (2.15a) neglect temperature effects, which can be included by adding the $\delta\mathcal{E}_{Varsh}$ term. A comparison of the effect of strain on $\mathrm{In}_x\mathrm{Ga}_{1-x}\mathrm{As}$ and $\mathrm{Al}_{1-x}\mathrm{In}_x\mathrm{As}$ bandgaps is shown in Fig. 2.3.

2.3 Effective Mass

Just as important as the potential profile to accurate solutions of the Schrödinger equation is the effective mass. Fundamentally, the effective mass of an individual energy band is influenced by the surrounding energy bands. Using $\mathbf{k}\bullet\mathbf{p}$ theory, the conduction band effective mass perpendicular to the plane of epitaxial growth $m^*\left(z,\mathcal{E}_q\right)$ can be derived as [27], [29], [38]

$$\frac{1}{m^*\left(z,\mathcal{E}_q\right)} = \frac{1}{m_0}\left\{1 + 2F + \frac{\mathcal{E}_P}{3}\left[\frac{\left(\sqrt{2}u - v\right)^2}{\mathcal{E}_q + \mathcal{E}^{\Gamma}_{\mathrm{C-LH}}} + \frac{\left(\sqrt{2}v + u\right)^2}{\mathcal{E}_q + \mathcal{E}^{\Gamma}_{\mathrm{C-SO}}}\right]\right\} \tag{2.17}$$

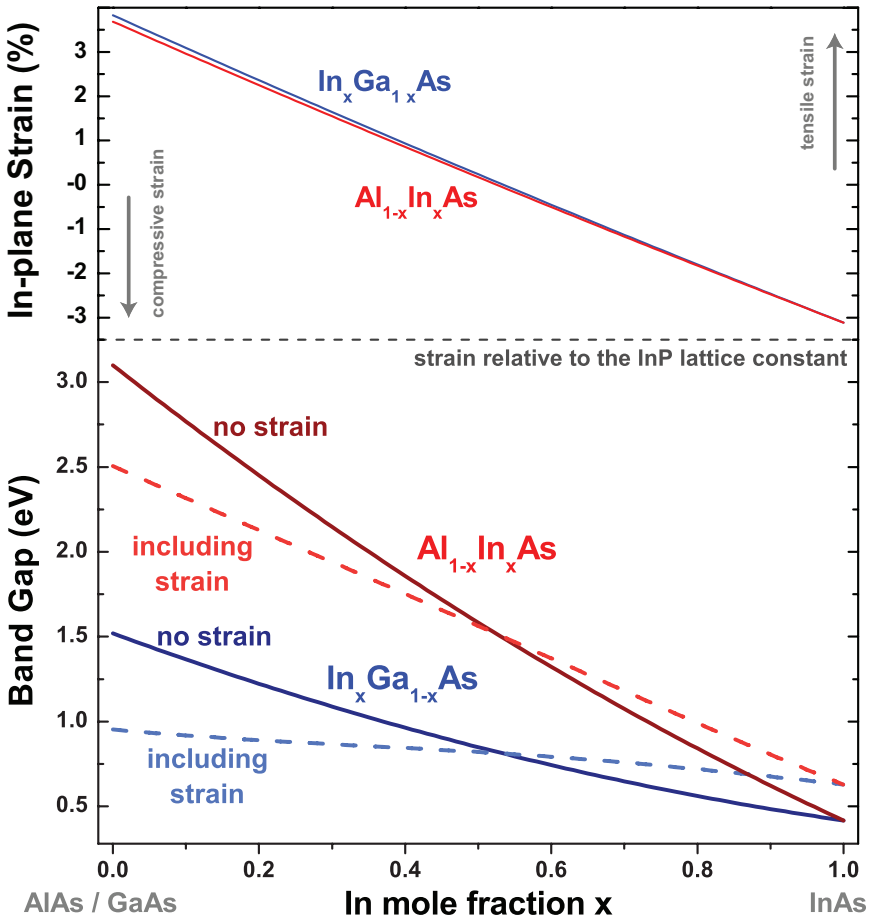

Figure 2.3: Bandgap strain dependence. The top panel shows in-plane strain ε_{xx} relative to the InP lattice constant (at 300 K) for $In_xGa_{1-x}As$ and $Al_{1-x}In_xAs$ of mole fraction x. The bottom panel compares the effect of strain on bandgap for the same materials compositions. Bandgap calculations where strain is ignored—that is, bandgaps only dependent upon material compositions—are shown as solid lines. (Here, $\mathcal{E}^{\Gamma}_{\mathrm{C-LH}}$ and $\mathcal{E}^{\Gamma}_{\mathrm{C-HH}}$ are degenerate when strain is zero.) Calculations for $\mathcal{E}^{\Gamma}_{\mathrm{C-LH}}$ that apply a correction for in-plane strain are shown as dashed lines. The correction $\delta\mathcal{E}_{Varsh}$ is not included here.

where each of the terms F, $\mathcal{E}_P$, u, v, $\mathcal{E}_q$, $\mathcal{E}^{\Gamma}_{\mathrm{C-LH}}$, and $\mathcal{E}^{\Gamma}_{\mathrm{C-SO}}$ have z-dependence. The free electron mass is m_0, F is the Kane parameter representing the second-order $\mathbf{k}\bullet\mathbf{p}$ perturbation term, $\mathcal{E}_P$ is the energy-unit representation of the momentum matrix element between the s-like conduction bands and p-like valence bands, $\mathcal{E}_q$ is the energy of the quantized energy state above or below the conduction band, and u and

v represent the degree of mixing between LH and SO states and are give as

$$u = \frac{2\sqrt{2}|Q_\varepsilon|}{C} \qquad \text{and} \qquad v = \frac{(A-B)|Q_\varepsilon|}{CQ_\varepsilon} \tag{2.18}$$

with

$$A = \Delta_{\text{SO}} + Q_\varepsilon\,, \quad B = \sqrt{\Delta_{\text{SO}}^2 + 2\Delta_{\text{SO}}Q_\varepsilon + 9Q_\varepsilon^2}\,, \quad \text{and} \quad C = \sqrt{2B(B-A)}\,. \tag{2.19}$$

In the case of no strain, $u = 1$ and $v = 0$. Moreover, for in-plane strain values up to ~2%, $u \approx 1$ and $v \approx 0$ so

$$\frac{1}{m^*\left(z, \mathcal{E}_q\right)} = \frac{1}{m_0}\left\{1 + 2F + \frac{\mathcal{E}_P}{3}\left[\frac{2}{\mathcal{E}_q + \mathcal{E}_{\text{C-LH}}^\Gamma} + \frac{1}{\mathcal{E}_q + \mathcal{E}_{\text{C-SO}}^\Gamma}\right]\right\} \tag{2.20}$$

is a good approximation. Both $\mathcal{E}_P$ and F are well-reviewed for III–V materials by Vurgaftman *et al.* [29], and they are generally considered to be independent of strain and temperature. Using Eq. (2.17) or (2.20), the energy dependence of the effective mass in a quantum well (*i.e.* non-parabolicity) [27], [39] is taken into account by virtue of $\mathcal{E}_q$. Also, the effects of strain and temperature on effective mass are accounted for by their effects on the bandgaps $\mathcal{E}_{\text{C-LH}}^\Gamma$ and $\mathcal{E}_{\text{C-SO}}^\Gamma$.

2.4 Self-consistent Solutions of the Schrödinger and Poisson Equations

Knowing the energy gaps and band offsets of our materials system, we can calculate the semiconductor material potential profile $V_{mat}(z)$. However, when semiconductors are doped, the fixed and free charges (ionized impurities and free electrons, respectively) that make up a charge distribution ρ add a perturbation to the potential profile. Given by the Poisson equation, this perturbation V_ρ is

$$\nabla^2 V_\rho = -\frac{\rho}{\epsilon} \tag{2.21}$$

where $\epsilon = \epsilon_r \epsilon_0$ is the material permittivity. The potential $V_\rho(z)$ can otherwise be found through the electric field strength $E(z)$:

$$V_\rho(z) = \int_{-\infty}^{z} E(z)\, dz\,. \tag{2.22}$$

With our system of energy states quantized in one dimension (z), and our wavefunctions $\psi(z)$ numerically solved at discrete points with spacing δz, we can think of the charge density $\rho(z)$ as infinite sheets, with sheet density $\sigma(z)$ and thickness δz (similar to the process outlined by Harrison [28]). The resultant perpendicular electric field to an infinite plane of charge is

$$E = \frac{\sigma}{2\epsilon} \tag{2.23}$$

and we can thus sum the contributions to the aggregate electric field from all of the individual "slices" of δz as

$$E(z) = -\sum_{z'=-\infty}^{z-\delta z} \frac{\sigma(z')}{2\epsilon} + \sum_{z'=z}^{\infty} \frac{\sigma(z')}{2\epsilon} \tag{2.24}$$

which accounts for the sign of the field being dependent on the location of the position z relative to the position of the charge slice z'. The sheet charge density $\sigma(z)$ includes both negative free electron charge and positive ionized impurity charge. For a doping density profile $N_d(z)$ $[\frac{1}{\text{volume}}]$, the total free electron sheet density n_s $[\frac{1}{\text{area}}]$ will be given by

$$n_s = \int_{-\infty}^{+\infty} N_d(z)\, dz \tag{2.25}$$

and the fixed charge sheet density is $N_d(z)\delta z$. The net sheet charge density is thus

$$\sigma(z) = q\left[N_d(z)\delta z - n_s \psi_i^*(z)\psi_i(z)\right] \tag{2.26}$$

where q is the absolute value of the electron charge ($q = |q|$). It is imiportant to note that Eq. (2.26) holds only if all free electrons are in the quantum state i. If all electrons are not in a single quantum state (*i.e.* $T \neq 0$ K), we can distribute them over the set of relevant states using the Fermi distribution as a weighting function. For the quantum state i at

energy $\mathcal{E}_i$, the Fermi distribution is

$$f(\mathcal{E}_i) = \frac{1}{e^{\frac{(\mathcal{E}_i - \mathcal{E}_0) - \mathcal{E}_F(T)}{k_B T}} + 1} \tag{2.27}$$

where $\mathcal{E}_0$ is the energy of the lowest state in the QC period (the injector ground state, for example) and $\mathcal{E}_F(T)$ is the Fermi energy at temperature T given by [40]

$$\mathcal{E}_F(T) = k_B T \ln\left(e^{\frac{\mathcal{E}_F(0)}{k_B T}} - 1\right) \tag{2.28}$$

and

$$\mathcal{E}_F(0) = n_s \frac{\pi\hbar^2}{m^*} . \tag{2.29}$$

Now, for n_s electrons thermally distributed over quantum states 1 through n, the population in state i can be determined by the weighting coefficient ξ_i such that

$$\xi_i = \frac{f(\mathcal{E}_i)}{\sum_{i=1}^{n} f(\mathcal{E}_i)} \tag{2.30}$$

and

$$n_i = \xi_i n_s \tag{2.31}$$

so long as we ensure that the individual weighting coefficients sum to one $\left(\sum_{i=1}^{n} \xi_i = 1\right)$. Our sheet charge density now becomes

$$\sigma(z) = q\left[N_d(z)\delta z - \sum_{i=1}^{n} \xi_i n_s \psi_i^*(z)\psi_i(z)\right] \tag{2.32}$$

for the electron-occupied set of quantum states 1 through n.

Following the above procedure to find the charge potential V_ρ, we can apply this correction as a perturbation to the overall potential: $V_C(z) = V_{mat}(z) + V_\rho(z)$. We can then solve our system using Eq. (2.6) and the shooting method described previously with the new composite potential. Certainly, the perturbation from V_ρ changes the solution to the system enough that a new V_ρ can be calculated based on the shifted electron wavefunctions. Thus, an iterative approach is needed, where V_ρ is updated after each iteration until consecutive solutions converge. Ergo, a self-consistent solution.

2.5 Spontaneous Emission Rate and the Optical Dipole Matrix Element

The optical transition rate W_{opt} between two eigen states of a system, such as an upper state ψ_{C}^{u} and lower state ψ_{C}^{ℓ}, is given by first order perturbation theory (Fermi's golden rule) as [41]

$$W_{opt}^{\vec{k},\vartheta} = \frac{2\pi}{\hbar}|\langle\psi_{\mathrm{C}}^{\ell},\mathcal{N}_{\vec{k},\vartheta}^{\ell}|\mathscr{H}'|\psi_{\mathrm{C}}^{u},\mathcal{N}_{\vec{k},\vartheta}^{u}\rangle|^2\delta(\mathcal{E}_u-\mathcal{E}_\ell-\mathcal{E}_{\vec{k}}) \tag{2.33}$$

for the optical mode with wavevector $\vec{k}$ and polarization ϑ, where the interaction Hamiltonian $\mathscr{H}'$ is the light–matter perturbation responsible for the transition and the terms $\mathcal{N}_{\vec{k},\vartheta}^{u}$ and $\mathcal{N}_{\vec{k},\vartheta}^{\ell}$ represent quantized states (number of photons) of the electromagnetic field. The total Hamiltonian that includes the light–matter interaction for an electron in the conduction band is given as [41]

$$\mathscr{H} = \frac{\left(\vec{\mathcal{P}}-q\boldsymbol{A}\right)^2}{2m^*} + qV_{\mathrm{C}}(\vec{r}) \tag{2.34}$$

where $\vec{\mathcal{P}}$ is the momentum operator in three dimensions, $\vec{r}$ is a position vector, and assuming for the moment a constant effective mass m^*. Taking $\boldsymbol{A}$ to be the vector potential of the optical field in the Coulomb gauge so that $\nabla\cdot\boldsymbol{A}=0$, Eq. (2.34) becomes

$$\mathscr{H} = \frac{\vec{\mathcal{P}}^2}{2m^*} - \frac{q}{m^*}\left(\boldsymbol{A}\cdot\vec{\mathcal{P}}\right) + \frac{q^2}{2m^*}A^2 + qV_{\mathrm{C}}(\vec{r}) \tag{2.35}$$

after also using the commutation $[\vec{\mathcal{P}},\boldsymbol{A}]=0$ for the Coulomb gauge [41]. We may assume that the term in A^2 is negligible given sufficiently small optical field intensity and matrix elements of $\vec{\mathcal{P}}$ [42]; that is, we ignore two photon processes [43]. Thus, our interaction Hamiltonian $\mathscr{H}'$ is

$$\mathscr{H}' = -\frac{q}{m^*}\left(\boldsymbol{A}\cdot\vec{\mathcal{P}}\right) \tag{2.36}$$

given that the remainder of Eq. (2.35) is the unperturbed Hamiltonian

$$\mathscr{H}_0 = \frac{\vec{\mathcal{P}}^2}{2m^*} + qV_{\mathrm{C}}(\vec{r})\,. \tag{2.37}$$

Applying Eq. (2.36) to Eq. (2.33), the optical transition rate is

$$W_{opt}^{\vec{k},\vartheta} = \frac{2\pi}{\hbar}\frac{q^2}{m^{*2}}|\langle\psi_{\mathrm{C}}^{\ell},\mathcal{N}_{\vec{k},\vartheta}^{\ell}|\boldsymbol{A}\cdot\vec{\mathcal{P}}|\psi_{\mathrm{C}}^{u},\mathcal{N}_{\vec{k},\vartheta}^{u}\rangle|^2\delta(\mathcal{E}_u-\mathcal{E}_\ell-\mathcal{E}_{\vec{k}})\,. \tag{2.38}$$

The operator form of the vector potential $\boldsymbol{A}$ is derived using a plane wave expansion for a cavity with mode volume $\mathcal{V}_{\vec{k}}$ and permittivity ϵ as [43]

$$\boldsymbol{A}(\vec{r}) = \sum_{\vec{k},\vartheta}\sqrt{\frac{\hbar}{2\epsilon\omega_{\vec{k}}\mathcal{V}_{\vec{k}}}}\left[\hat{b}_{\vec{k},\vartheta}^{\dagger}e^{-i\vec{k}\cdot\vec{r}}+\hat{b}_{\vec{k},\vartheta}e^{i\vec{k}\cdot\vec{r}}\right]\hat{e}_{\vec{k},\vartheta} \tag{2.39}$$

where $\hat{e}_{\vec{k},\vartheta}$ is the unit vector for the photon mode, $\hat{b}_{\vec{k},\vartheta}^{\dagger}$ and $\hat{b}_{\vec{k},\vartheta}$ are the photon creation and annihilation operators, and the term $\sqrt{\frac{\hbar}{2\epsilon\omega_{\vec{k}}}}$ provides MKS units. We now invoke the dipole approximation, which treats the photon wavelength as being large compared to the space over which the optical transition occurs [43]. One result of the dipole approximation—with $|\vec{k}|=\frac{2\pi}{\lambda}\approx 10^6$ m^{-1} and the electron confinement space in the QC active region $|\vec{r}|\approx 10^{-8}$ m—is that $e^{i\vec{k}\cdot\vec{r}}\approx 1$. Also, using the relation $\mathcal{N}_{\vec{k},\vartheta}^{\ell}=\mathcal{N}_{\vec{k},\vartheta}^{u}+1$ since a photon is created in the transition $|\psi_{\mathrm{C}}^{u}\rangle\rightarrow|\psi_{\mathrm{C}}^{\ell}\rangle$,

$$\langle\mathcal{N}_{\vec{k},\vartheta}^{u}+1|\hat{b}_{\vec{k},\vartheta}^{\dagger}|\mathcal{N}_{\vec{k},\vartheta}^{u}\rangle=\sqrt{\mathcal{N}_{\vec{k},\vartheta}^{u}+1}\langle\mathcal{N}_{\vec{k},\vartheta}^{u}+1|\mathcal{N}_{\vec{k},\vartheta}^{u}+1\rangle=\sqrt{\mathcal{N}_{\vec{k},\vartheta}^{u}+1} \tag{2.40a}$$

and

$$\langle\mathcal{N}_{\vec{k},\vartheta}^{u}+1|\hat{b}_{\vec{k},\vartheta}|\mathcal{N}_{\vec{k},\vartheta}^{u}\rangle=\sqrt{\mathcal{N}_{\vec{k},\vartheta}^{u}}\langle\mathcal{N}_{\vec{k},\vartheta}^{u}+1|\mathcal{N}_{\vec{k},\vartheta}^{u}-1\rangle=0\,. \tag{2.40b}$$

Finally, we can make the approximation that $\vec{\mathcal{P}}$ affects only the electron momentum, which is accurate in our low photon field approximation. In this case, $\boldsymbol{A}\cdot\vec{\mathcal{P}}$ is separable so that $\langle\psi_{\mathrm{C}}^{\ell}|\vec{\mathcal{P}}|\psi_{\mathrm{C}}^{u}\rangle\cdot\langle\mathcal{N}_{\vec{k},\vartheta}^{\ell}|\boldsymbol{A}|\mathcal{N}_{\vec{k},\vartheta}^{u}\rangle$ and Eq. (2.38) becomes

$$W_{opt}^{\vec{k},\vartheta} = \frac{\pi q^2}{\epsilon m^{*2}\mathcal{V}_{\vec{k}}}\frac{\left(\mathcal{N}_{\vec{k},\vartheta}^{u}+1\right)}{\omega_{\vec{k}}}|\hat{e}_{\vec{k},\vartheta}\cdot\langle\psi_{\mathrm{C}}^{\ell}|\vec{\mathcal{P}}|\psi_{\mathrm{C}}^{u}\rangle|^2\delta(\mathcal{E}_u-\mathcal{E}_\ell-\mathcal{E}_{\vec{k}}) \tag{2.41}$$

for a single optical mode. Now, by applying the commutation relation [41]

$$\vec{\mathcal{P}} = \frac{im^*}{\hbar}[\mathscr{H}_0, \vec{r}] \tag{2.42}$$

we get

$$\langle \psi_{\mathrm{C}}^{\ell} | \vec{\mathcal{P}} | \psi_{\mathrm{C}}^{u} \rangle = \frac{im^*}{\hbar} \langle \psi_{\mathrm{C}}^{\ell} | \mathscr{H}_0 \cdot \vec{r} - \vec{r} \cdot \mathscr{H}_0 | \psi_{\mathrm{C}}^{u} \rangle = im^* \omega_0 \langle \psi_{\mathrm{C}}^{\ell} | \vec{r} | \psi_{\mathrm{C}}^{u} \rangle \tag{2.43}$$

and so

$$W_{opt}^{\vec{k},\vartheta} = \frac{\pi q^2}{\epsilon \mathcal{V}_{\vec{k}}} \left(\mathcal{N}_{\vec{k},\vartheta}^{u} + 1 \right) \omega_0 |\hat{e}_{\vec{k},\vartheta} \cdot \langle \psi_{\mathrm{C}}^{\ell} | \vec{r} | \psi_{\mathrm{C}}^{u} \rangle|^2 \delta(\mathcal{E}_u - \mathcal{E}_\ell - \mathcal{E}_{\vec{k}}) \,. \tag{2.44}$$

From here, we can distinguish two contributions to the optical transition rate: those of stimulated emission $W_{stim}^{\vec{k},\vartheta}$ due to the presence of an inducing field proportional to $\mathcal{N}_{\vec{k},\vartheta}^{u}$ and spontaneous emission $W_{spon}^{\vec{k},\vartheta}$ due to zero-point field such that

$$W_{opt}^{\vec{k},\vartheta} = W_{stim}^{\vec{k},\vartheta} + W_{spon}^{\vec{k},\vartheta} \,. \tag{2.45}$$

Since the wavefunctions ψ_{C}^{u} and ψ_{C}^{ℓ} have quantization only in the z direction, we can further simplify to

$$W_{stim}^{\vec{k},\vartheta} = \frac{\pi q^2}{\hbar \epsilon \mathcal{V}_{\vec{k}}} \omega_0 z_{u\ell}^2 |\hat{e}_{\vec{k},\vartheta} \cdot \hat{z}|^2 \delta(\omega_0 - \omega_{\vec{k}}) \mathcal{N}_{\vec{k},\vartheta}^{u} \tag{2.46a}$$

$$W_{spon}^{\vec{k},\vartheta} = \frac{\pi q^2}{\hbar \epsilon \mathcal{V}_{\vec{k}}} \omega_0 z_{u\ell}^2 |\hat{e}_{\vec{k},\vartheta} \cdot \hat{z}|^2 \delta(\omega_0 - \omega_{\vec{k}}) \tag{2.46b}$$

where $\hat{z}$ is the unit vector in the z direction, the optical dipole matrix element $z_{u\ell}$ is defined as

$$z_{u\ell} \equiv \langle \psi_{\mathrm{C}}^{\ell} | z | \psi_{\mathrm{C}}^{u} \rangle \tag{2.47}$$

and the transformation $\mathcal{E}_u - \mathcal{E}_\ell = \hbar\omega_0$ has been used.

Concentrating now just on the spontaneous emission, the total spontaneous emission rate is realized by summing over all modes in the optical cavity. Equivalently, we can integrate over the product of all possible modes and the density of the cavity photon modes $\mathscr{D}$.

$$W_{spon} = \sum_{\vec{k},\vartheta} W_{spon}^{\vec{k},\vartheta} = \int\int\int W_{spon}^{\vec{k},\vartheta} \times \mathscr{D}(\omega_{\vec{k}}) \, d^3\omega_{\vec{k}} \tag{2.48}$$

For an arbitrarily shaped electromagnetic enclosure where the dimensions are at least a few times the transition wavelength [44], the differential mode density $\mathscr{D}_{3D}(\omega_{\vec{k}})d^3\omega_{\vec{k}}$ is given in spherical coordinates as [45]

$$\mathscr{D}_{3D}(\omega_{\vec{k}})d^3\omega_{\vec{k}} = \frac{d^3\omega_{\vec{k}}}{\frac{8\pi^3}{\mathcal{V}_{\vec{k}}}} = \frac{\mathcal{V}_{\vec{k}}}{8\pi^3}k^2\sin\theta\, d\vec{k}\, d\theta\, d\phi = \frac{n_{eff}^3}{c_0^3}\frac{\mathcal{V}_{\vec{k}}}{8\pi^3}\omega_{\vec{k}}^2\sin\theta\, d\omega_{\vec{k}}\, d\theta\, d\phi \tag{2.49}$$

where n_{eff} is the effective refractive index of the mode, c_0 is the speed of light in vacuum, θ is the zenith angle from the positive z-axis, and ϕ is the azimuth angle from the positive x-axis. Combining Eqs. (2.46b) and (2.49) into Eq. (2.48) gives

$$W_{spon} = \frac{q^2 n_{eff}^3 \omega_0}{8\pi^2\hbar\epsilon c_0^3} z_{u\ell}^2 \int_0^\infty \omega_{\vec{k}}^2 \delta(\omega_0 - \omega_{\vec{k}}) d\omega_{\vec{k}} \int_0^{2\pi}\int_0^{\pi} |\hat{e}_{\vec{k},\vartheta}\cdot\hat{z}|^2 \sin\theta d\theta d\phi\,. \tag{2.50}$$

For the two orthogonal polarizations $\hat{e}_{\vec{k},\vartheta=1}$ and $\hat{e}_{\vec{k},\vartheta=2}$, we can choose $\hat{e}_{\vec{k},\vartheta=1}$ to lie in the plane of $\hat{z}$ and k_z so that $|\hat{e}_{\vec{k},\vartheta=2}\cdot\hat{z}|^2 = 0$. Using $|\hat{e}_{\vec{k},\vartheta}\cdot\hat{z}|^2 = \sin^2\theta$ and $\epsilon = n_{eff}^2\epsilon_0$, the spontaneous emission rate is [42] [43] [44] [46]

$$W_{spon} = \frac{1}{\tau_{spon}} = \frac{q^2 n_{eff}\omega_0^3}{3\pi\hbar\epsilon_0 c_0^3} z_{u\ell}^2 \tag{2.51}$$

where τ_{spon} is the spontaneous emission lifetime.

Normalization of the wavefunctions ψ_c

To this point in our derivation of τ_{spon}, we have assumed an effective mass m^* that is constant with energy. We now appropriately account for the variable effective mass with proper normalization the wavefunctions ψ_c that are used to calculate our optical dipole matrix element $z_{u\ell}$.

In previous sections, our solutions for conduction band eigenstates ψ_c have used the envelope function Hamiltonian in the Kane approximation [47]. In the Kane approximation, the full system Hamiltonian is projected onto the individual subbands (conduction band, light hole band, etc.). If the in-plane electron momentum is assumed to vanish, the total stationary wavefunction is given by the three components ψ_c, ψ_{LH}, and ψ_{SO}, weighted with their corresponding Bloch functions [27]. Consequently, knowledge of

only the conduction component ψ_{C} is insufficient for the complete physical description of the stationary state, and the stationary state is thus normalized as [27]

$$\langle\psi_{\mathrm{C}}|\psi_{\mathrm{C}}\rangle + \langle\psi_{\mathrm{LH}}|\psi_{\mathrm{LH}}\rangle + \langle\psi_{\mathrm{SO}}|\psi_{\mathrm{SO}}\rangle = 1 \tag{2.52}$$

However, just as our calculation of the energy-dependent effective mass in Eq. (2.17) included the conduction band interaction with the valence bands, we can likewise recast Eq. (2.52) entirely in terms of ψ_{C} as [27]

$$\langle\psi_{\mathrm{C}}|1 + \frac{2}{3}\mathcal{P}_z\frac{\mathcal{E}_P}{2m_0\left(\mathcal{E}_q + \mathcal{E}^{\Gamma}_{\mathrm{LH}}\right)^2}\mathcal{P}_z + \frac{1}{3}\mathcal{P}_z\frac{\mathcal{E}_P}{2m_0\left(\mathcal{E}_q + \mathcal{E}^{\Gamma}_{\mathrm{SO}}\right)^2}\mathcal{P}_z|\psi_{\mathrm{C}}\rangle = 1\,. \tag{2.53}$$

Defining the average valence band energy as $\mathcal{E}_v = \frac{2\mathcal{E}_{\mathrm{LH}}+\mathcal{E}_{\mathrm{SO}}}{3}$, we may further simplify Eq. (2.53) and approximate it as [48]

$$\langle\psi_{\mathrm{C}}|1 + \frac{\mathcal{P}_z^2}{2m^*(\mathcal{E}_q)(\mathcal{E}_q + \mathcal{E}_v)}|\psi_{\mathrm{C}}\rangle = 1 \tag{2.54}$$

or equivalently

$$\langle\psi_{\mathrm{C}}|1 + \frac{\mathcal{E}_q}{\mathcal{E}_q + \mathcal{E}_v}|\psi_{\mathrm{C}}\rangle = 1\,. \tag{2.55}$$

2.6 Stimulated Emission Probability and the Transition Cross Section

In the previous section, we derived the probability of stimulated emission for a single optical mode $\vec{k}$ as

$$W^{\vec{k},\vartheta}_{stim} = \frac{\pi q^2}{\hbar\epsilon\mathcal{V}_{\vec{k}}}\omega_{\vec{k}}z^2_{u\ell}|\hat{e}_{\vec{k},\vartheta}\cdot\hat{z}|^2\delta(\omega_0 - \omega_{\vec{k}})\mathcal{N}^u_{\vec{k},\vartheta} \tag{2.56}$$

In general, the transition frequency ω_0 is not a single value, but is instead broadened. We thus substitute $\delta(\omega_0 - \omega_{\vec{k}})$ for the normalized Lorentzian lineshape function $\mathscr{L}(\nu)$ given as

$$\mathscr{L}(\nu) = \frac{\frac{\delta\nu}{2\pi}}{(\nu_0 - \nu)^2 + \left(\frac{\delta\nu}{2}\right)^2} \tag{2.57}$$

and then integrate over ν. Now, the stimulated emission probability becomes [42]

$$W_{stim}^{\vec{k},\vartheta} = \frac{\pi q^2 z_{u\ell}^2 \mathcal{N}_{\vec{k},\vartheta}}{h\mathcal{V}_{\vec{k}}\epsilon}\mathscr{L}(\nu) \tag{2.58}$$

We can also now relate the number of mode photons $\mathcal{N}_{\vec{k},\vartheta}$ to a photon mode flux ϕ_{ph} $[\frac{\text{photons}}{\text{area}\times\text{time}}]$ using the group velocity v_g where

$$\phi_{ph} = \frac{v_g}{\mathcal{V}_{\vec{k}}}\mathcal{N}_{\vec{k},\vartheta} \tag{2.59}$$

so that [42]

$$W_{stim} = \phi_{ph}\frac{3\lambda_0^2}{8\pi\tau_{spon}}\mathscr{L}(\nu) \tag{2.60}$$

where Eq. (2.51) is used to eliminate $z_{u\ell}^2$. The factor of 3 results from the polarization of the cavity mode [49]. Now, a useful quantity known as the transition cross section $\sigma(\nu)$ [area] and defined as [45]

$$W_{stim} = \phi_{ph}\sigma(\nu) \tag{2.61}$$

is given by

$$\sigma(\nu) = \frac{2\pi^2 q^2 \mathcal{E}_{ph}}{h^2 c\epsilon_0 n_{eff}} z_{u\ell}^2 \mathscr{L}(\nu) \tag{2.62}$$

and $\sigma(\nu_0) = \sigma_0$ where ν_0 is the lasing frequency at the photon energy $\mathcal{E}_{ph}$ is

$$\sigma_0 = \frac{4\pi q^2}{hc\epsilon_0 n_{eff}}\frac{\mathcal{E}_{ph}}{\delta\mathcal{E}_{u\ell}} z_{u\ell}^2 \,. \tag{2.63}$$

2.7 LO-phonon Scattering Time

The fastest scattering process between energy states within the same band of semiconductor quantum wells is the non-radiative longitudinal optical (LO) phonon transition [50]. Because it is the fastest transition process, quantifying the LO phonon lifetime becomes particularly relevant for QC laser design. Charge carrier interaction with the electric polarization produced by the relative displacement of the positive and negative ions of polar semiconductors is referred to as the Fröhlich interaction. The Fröhlich

Hamiltonian $\mathscr{H}_F$ is given as

$$\mathscr{H}_F = \sum_{\mathbf{Q}} \sqrt{\frac{2\pi\hbar\omega_{\mathrm{LO}} q^2}{(\epsilon_\infty - \epsilon_s)\mathcal{V}_Q Q^2}} e^{-i\mathbf{Q}\cdot\mathbf{r}} a_{\mathbf{Q}}^\dagger \tag{2.64}$$

where $\hbar\omega_{\mathrm{LO}}$ is the LO phonon energy, ϵ_∞ is the high frequency relative permittivity, ϵ_s is the static relative permittivity, $\mathcal{V}_Q$ is the volume of the system, Q is the magnitude of the phonon wavevector $\mathbf{Q}$, $\mathbf{r}$ is the position vector, and $a_{\mathbf{Q}}^\dagger$ is the creation operator for a phonon in the mode $\mathbf{Q}$. Using Fermi's golden rule, the LO phonon lifetime $\tau_{u\ell}$ between an initial (upper) state $|u,\mathbf{k}_u\rangle$ and final (lower) state $|\ell,\mathbf{k}_\ell\rangle$ with electron wavevector $\mathbf{k}$ at $T = 0$ K is then

$$\frac{1}{\tau_{u\ell}} = \frac{\sqrt{m^*(\mathcal{E}_u)\, m^*(\mathcal{E}_\ell)}\, q^2 \omega_{\mathrm{LO}}}{2\hbar^2(\epsilon_\infty - \epsilon_s)} \int_0^{2\pi} \frac{\int_{-\infty}^{+\infty}\int_{-\infty}^{+\infty} \psi_{\mathrm{C}}^u(z)\psi_{\mathrm{C}}^\ell(z) e^{-Q|z-z'|}\psi_{\mathrm{C}}^u(z')\psi_{\mathrm{C}}^\ell(z')\, dz\, dz'}{Q} \sin\theta\, d\theta \tag{2.65}$$

where Q is given by

$$Q = \sqrt{k_u^2 + k_\ell^2 - 2k_u k_\ell \cos\theta} \tag{2.66}$$

and k_u and k_ℓ are related by

$$k_\ell^2 = \frac{m^*(\mathcal{E}_\ell)}{m^*(\mathcal{E}_u)} k_u^2 + \frac{2m^*(\mathcal{E}_\ell)}{\hbar^2}(\mathcal{E}_{u\ell} - \hbar\omega_{\mathrm{LO}}) \ . \tag{2.67}$$

If we assume the electron initially starts at wavevector $k_u = 0$, then

$$k_\ell = \sqrt{\frac{2m^*(\mathcal{E}_\ell)}{\hbar^2}(\mathcal{E}_{u\ell} - \hbar\omega_{\mathrm{LO}})} \tag{2.68}$$

and $Q = k_\ell$ so Eq. (2.65) simplifies to

$$\frac{1}{\tau_{u\ell}} = \frac{\sqrt{m^*(\mathcal{E}_u)\, m^*(\mathcal{E}_\ell)}\, q^2 \omega_{\mathrm{LO}}}{2\hbar^2(\epsilon_\infty - \epsilon_s)} \int_{-\infty}^{+\infty}\int_{-\infty}^{+\infty} \frac{\psi_{\mathrm{C}}^u(z)\psi_{\mathrm{C}}^\ell(z) e^{-k_\ell|z-z'|}\psi_{\mathrm{C}}^u(z')\psi_{\mathrm{C}}^\ell(z')}{k_\ell}\, dz\, dz' \ . \tag{2.69}$$

The temperature dependence of $\tau_{u\ell}$ is attained by modifying the $T = 0$ K rate using the Bose–Einstein occupation number for phonons of energy $\hbar\omega_{\mathrm{LO}}$. Specifically, taking

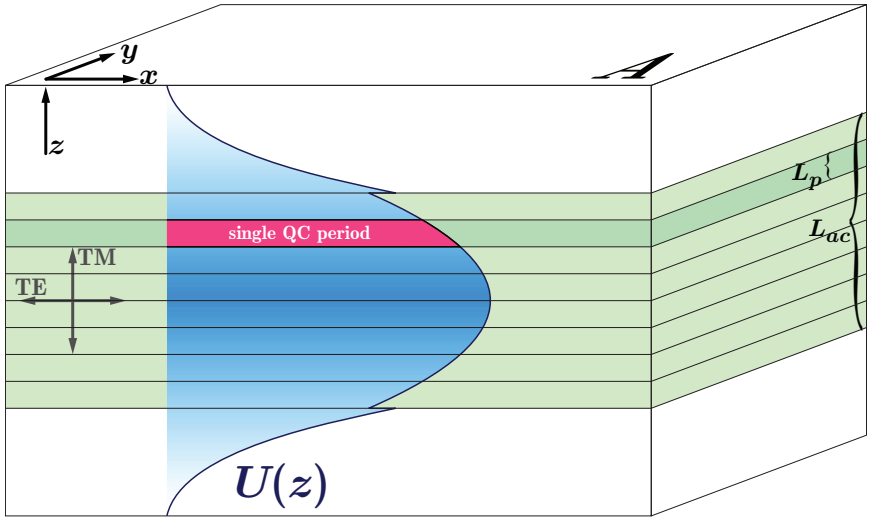

Figure 2.4: Sketch of waveguide geometry. A one dimensional optical mode profile (TM polarization) is shown as $U(z)$. Multiple QC periods with higher refractive index than the surrounding cladding confine the mode, and the reduced field intensity for off-center QC periods is seen. The arrows labeled TM and TE show direction of the electric field vector for the respective polarization.

into account both phonon emission and absorption processes [50],

$$\frac{1}{\tau_{u\ell}(T)} = \frac{1}{\tau_{u\ell}(0)}\left(1 + \frac{2}{e^{\frac{\hbar\omega_{\mathrm{LO}}}{k_{\mathrm{B}}T}} - 1}\right). \tag{2.70}$$

2.8 Rate Equations for QC Lasers

Rate equations are a phenomenological method for describing laser devices from which important performance parameters (*e.g.* output power, wall-plug efficiency, threshold, etc.) can be derived. Before directly discussing rate equations for QC lasers, it is important to recognize some of their unique properties. These properties extend from the fact that QC lasers have multiple active–injector region periods of gain region within the QC core, and each individual period can have its own local properties of photon field intensity and temperature; each period can furthermore have individually-customized emission [51] and doping profiles [52] that can be treated accordingly by the rate equations. In the following discussion, we restrict ourselves to the case where the design

of individual QC periods is identical. In this case, we must concern ourselves only with the local field intensity and the local electron populations for each period.

In semiconductor lasers, field intensities in the gain region are usually treated through the use of confinement factor Γ, which is defined for the 1D case as [53]

$$\Gamma = \frac{\int_{z_0}^{z_0+L_{ac}} n_r(z)U(z)\,dz}{\int_{-\infty}^{+\infty} n_r(z)U(z)\,dz} \tag{2.71}$$

where z_0 marks the beginning of the active core, L_{ac} is the thickness of the active core, $n_r(z)$ is the refractive index profile, and $U(z)$ is the dimensionless mode intensity profile normalized such that $\max(U(z)) = 1$. The mode profile $U(z)$ can also be used to identify an "effective mode volume" $\mathcal{V}_{ph}$, here for the 1D case, such that

$$\mathcal{V}_{ph} = A\int_{-\infty}^{+\infty} U(z)\,dz \tag{2.72}$$

where A is the device area in the x and y dimensions, and so that the active core volume $\mathcal{V}_{ac} = AL_{ac}$. We now also have a 1D "mode thickness" L_{ph} analogous to the active core thickness L_{ac} given as

$$L_{ph} = \int_{-\infty}^{+\infty} U(z)\,dz\,. \tag{2.73}$$

In the typical set of rate equations describing diode lasers, which do not address the QC feature of a multiple gain region stack, it is commonly assumed that the gain profile is a square function over the active region, and so $\Gamma = \frac{L_{ac}}{L_{ph}}$; here, the refractive index profile $n_r(z)$ is also assumed to be constant. We will not make these assumptions in the following rate equation analysis for QC structures. Instead, we will use a "local field coefficient" $\bar{U}_i$ for an individual QC period i given as

$$\bar{U}_i = \frac{\int_{z_i}^{z_i+L_p} n_r(z)U(z)\,dz}{\int_{z_i}^{z_i+L_p} n_r(z)\,dz} \tag{2.74}$$

where z_i marks the beginning of the QC period. For a QC structure with N_p identical periods, we have an active-injector period thickness L_p such that $L_{ac} = N_pL_p$ and an active-injector period volume $\mathcal{V}_p$ such that $\mathcal{V}_{ac} = N_p\mathcal{V}_p$. If the active period thickness

L_p is sufficiently thin, $\bar{U}_i \approx U(z_i)$. We can relate $\bar{U}_i$ to Γ by summing $\bar{U}_i$ over all N_p.

$$\Gamma = \frac{L_{ac}\sum_{i=1}^{N_p}\bar{U}_i}{L_{ph}} \tag{2.75}$$

In QC structures, the local electron populations can be individually affected by such things as the local field intensity and the local temperature. Thus, in the following analysis, we will treat the energy state populations of each QC period individually. Describing the change with respect to time in the upper state population $\mathcal{N}_{u,i}$, lower state population $\mathcal{N}_{\ell,i}$, and *total* photon population $\mathcal{N}_{ph}$ of the system gives the system of equations,

$$\mathcal{N}_{u,i}\,{}^{change}_{\text{w.r.t. time}} = {}^{\text{non-radiative}}_{\text{rate in}} - {}^{\text{non-radiative}}_{\text{rate out}} - {}^{\text{radiative}}_{\text{transition rate}} \tag{2.76a}$$

$$\mathcal{N}_{\ell,i}\,{}^{change}_{\text{w.r.t. time}} = {}^{\text{non-radiative}}_{\text{rate in}} - {}^{\text{non-radiative}}_{\text{rate out}} + {}^{\text{radiative}}_{\text{transition rate}} \tag{2.76b}$$

$$\mathcal{N}_{ph}\,{}^{change}_{\text{w.r.t. time}} = {}^{\text{sum over}}_{\text{all QC periods}}\left({}^{\text{radiative}}_{\text{transition rate}}\right) - {}^{\text{photon}}_{\text{loss rate}} \tag{2.76c}$$

where non-radiative transition rates are given by the population of the state $\mathcal{N}_{x,i}$ divided by the non-radiative lifetime τ_x for the energy state x. Radiative transition rates are given by

$${}^{\text{radiative}}_{\text{transition rate}} = \left({}^{\text{population}}_{\text{available for}}_{\text{stimulated emission}} - {}^{\text{population}}_{\text{available for}}_{\text{absorption}}\right) \times {}^{\text{probability of}}_{\text{stimulated emission}}$$

and

$${}^{\text{probability of}}_{\text{stimulated emission}} = {}^{\text{photon}}_{\text{density}} \times {}^{\text{photon}}_{\text{speed}} \times {}^{\text{transition}}_{\text{cross-section}} \times {}^{\text{local field}}_{\text{strength of mode}} .$$

Now, making Eq. (2.76) more explicit, our QC laser rate equations are thus generally expressed as

$$\frac{d\mathcal{N}_{u,i}}{dt} = \eta_{inj}\frac{I}{q} - \frac{\mathcal{N}_{u,i}}{\tau_u} - \left(\mathcal{N}_{u,i} - \mathcal{N}_{\ell,i}\right)\frac{\mathcal{N}_{ph}}{\mathcal{V}_{ph}} v_g \sigma_i \bar{U}_i \tag{2.77a}$$

$$\frac{d\mathcal{N}_{\ell,i}}{dt} = \frac{\mathcal{N}_{u,i}}{\tau_{u\ell}} - \frac{\mathcal{N}_{\ell,i}}{\tau_\ell} + \left(\mathcal{N}_{u,i} - \mathcal{N}_{\ell,i}\right)\frac{\mathcal{N}_{ph}}{\mathcal{V}_{ph}} v_g \sigma_i \bar{U}_i \tag{2.77b}$$

$$\frac{d\mathcal{N}_{ph}}{dt} = \sum_{i=1}^{N_p}\left[\left(\mathcal{N}_{u,i} - \mathcal{N}_{\ell,i}\right)\frac{\mathcal{N}_{ph}}{\mathcal{V}_{ph}} v_g \sigma_i \bar{U}_i\right] - \frac{\mathcal{N}_{ph}}{\tau_{ph}} \tag{2.77c}$$

where $\eta_{inj}\frac{I}{q}$ is the pumping rate for the upper laser state, τ_{ph} is the photon lifetime in the cavity, σ_i is the transition cross-section for the period i, and N_p is the total number of QC periods. The group velocity v_g is approximated by the phase velocity c_0/n_{eff}, which is accurate when dispersion is low. Rate equations are more traditionally represented int terms of population density $N\left[\frac{1}{\text{volume}}\right]$ rather than the absolute population $\mathcal{N}$ as above, so that we have

$$\frac{dN_{u,i}}{dt} = \eta_{inj}\frac{I}{q\mathcal{V}_p} - \frac{N_{u,i}}{\tau_u} - \left(N_{u,i} - N_{\ell,i}\right) N_{ph} v_g \sigma_0 \bar{U}_i \tag{2.78a}$$

$$\frac{dN_{\ell,i}}{dt} = \frac{N_{u,i}}{\tau_{u\ell}} - \frac{N_{\ell,i}}{\tau_\ell} + \left(N_{u,i} - N_{\ell,i}\right) N_{ph} v_g \sigma_0 \bar{U}_i \tag{2.78b}$$

$$\frac{dN_{ph}}{dt} = v_g \sigma_0 N_{ph}\frac{\mathcal{V}_{ac}}{\mathcal{V}_{ph}}\sum_{i=1}^{N_p}\left[\left(N_{u,i} - N_{\ell,i}\right)\bar{U}_i\right] - \frac{N_{ph}}{\tau_{ph}} \tag{2.78c}$$

where electron populations $\mathcal{N}_u$ and $\mathcal{N}_\ell$ in Eq. (2.77) were divided by the active core gain region volume $\mathcal{V}_{ac} = AL_{ac}$, the photon population $\mathcal{N}_{ph}$ divided by $\mathcal{V}_{ph}$, and we assume QC periods with identical design, so that $\sigma_i = \sigma_0$. Note that traditionally for diode lasers, $N_p = 1$, $\bar{U}_i = 1$, and $\Gamma = \frac{\mathcal{V}_{ac}}{\mathcal{V}_{ph}}$, so we recover the conventionally-written rate equations [35] [53] in that case.

For QC lasers, it is sometimes convenient to work with energy level populations in terms of sheet density $n\left[\frac{1}{\text{area}}\right]$ such that $n_i = N_i L_p$. It is also common to work in terms of photon flux photon flux $\phi_{ph}\left[\frac{1}{\text{area}\times\text{time}}\right]$ instead of photon density $N_{ph}\left[\frac{1}{\text{volume}}\right]$, so $N_{ph} = \frac{\phi_{ph}}{v_g}$.

$$\frac{dn_{u,i}}{dt} = \eta_{inj}\frac{J}{q} - \frac{n_{u,i}}{\tau_u} - \left(n_{u,i} - n_{\ell,i}\right)\phi_{ph}\sigma_0\bar{U}_i \tag{2.79a}$$

$$\frac{dn_{\ell,i}}{dt} = \frac{n_{u,i}}{\tau_{u\ell}} - \frac{n_{\ell,i}}{\tau_\ell} + \left(n_{u,i} - n_{\ell,i}\right)\phi_{ph}\sigma_0\bar{U}_i \tag{2.79b}$$

$$\frac{d\phi_{ph}}{dt} = v_g\sigma_0\phi_{ph}\frac{1}{L_{ph}}\sum_{i=1}^{N_p}\left[\left(n_{u,i} - n_{\ell,i}\right)\bar{U}_i\right] - \frac{\phi_{ph}}{\tau_{ph}} \tag{2.79c}$$

2.9 Threshold Current & Modal Gain

Using our rate equations in Eq. (2.79), we can solve for threshold current density J_{th} by taking steady state solutions of the rate equations $\left(\frac{d(\,)}{dt} = 0\right)$ and taking $\phi_{ph} = 0$. Applied to Eq. (2.79c), we find

$$\sum_{i=1}^{N_p}\left[\left(n_{u,i} - n_{\ell,i}\right)\right] = \frac{1}{\tau_{ph}v_g\sigma_0\frac{1}{L_{ph}}\sum_{i=1}^{N_p}\bar{U}_i} \tag{2.80}$$

which can be simplified to

$$n_u - n_\ell = \frac{L_{ac}}{\tau_{ph}v_g\sigma_0 N_p\Gamma} \tag{2.81}$$

if we now make the assumption of identical populations among all QC periods and incorporate Eq. (2.75). Now again taking the steady state solutions and $\phi_{ph} = 0$ for Eqs. (2.79a) and (2.79b), we yield our population inversion in terms of pumping rate and non-radiative lifetimes.

$$n_u - n_\ell = \eta_{inj}\frac{J}{qL_p}\tau_u\left(1 - \frac{\tau_\ell}{\tau_{u\ell}}\right) \tag{2.82}$$

which is our population inversion in terms of pumping rate R_{pump} where

$$R_{pump} = \eta_{inj}\frac{J}{qL_p} \tag{2.83}$$

and the effective upper state non-radiative lifetime τ_{eff} where

$$\tau_{eff} = \tau_u\left(1 - \frac{\tau_\ell}{\tau_{u\ell}}\right). \tag{2.84}$$

Combining Eqs. (2.81) and (2.82), our threshold current density is

$$J_{th} = \frac{qL_{ac}}{\eta_{inj}\tau_{eff}} \frac{1}{\tau_{ph} v_g \sigma_0 N_p \Gamma} \tag{2.85}$$

where a number of substitutions and simplifications will be useful. The photon lifetime τ_{ph} can be given in terms of the mirror loss α_m and waveguide loss α_w $[\frac{1}{\text{length}}]$

$$\frac{1}{\tau_{ph}} = v_g(\alpha_m + \alpha_w) \tag{2.86}$$

or equivalently in terms of total loss α_{tot} where $\alpha_{tot} = \alpha_m + \alpha_w$. We also take $\eta_{inj} = 1$ and apply Eq. (2.63) for σ_0 to arrive at

$$J_{th} = \frac{\alpha_m + \alpha_w}{\frac{4\pi q}{hc_0\epsilon_0 n_{eff}} \frac{\mathcal{E}_{u\ell}}{\delta\mathcal{E}_{u\ell}} \frac{1}{L_p} \tau_{eff} z_{u\ell}^2 \Gamma} . \tag{2.87}$$

Threshold current density is often simplified by incorporating a gain coefficient g $[\frac{\text{length}}{\text{current}}]$ given as

$$g = \frac{4\pi q}{hc_0\epsilon_0 n_{eff}} \frac{\mathcal{E}_{u\ell}}{\delta\mathcal{E}_{u\ell}} \frac{1}{L_p} \tau_{eff} z_{u\ell}^2 \tag{2.88}$$

or equivalently

$$g = \sigma_0 \frac{\tau_{eff}}{qL_p} \tag{2.89}$$

so that

$$J_{th} = \frac{\alpha_m + \alpha_w}{g\Gamma} . \tag{2.90}$$

Another common way to represent gain is as as modal gain γ [length] defined such that light intensity $\mathcal{I}$ after some distance L is given by

$$\mathcal{I}(L) = \mathcal{I}(0) e^{\gamma\Gamma L} \tag{2.91}$$

which is also equivalent to $\alpha_m + \alpha_w = \gamma\Gamma$ due to gain clamping [45]. Thus, given in terms of the threshold pumping current J_{th} and the transition cross-section σ_0, modal gain is

$$\gamma = J_{th} g = \frac{J_{th}}{qL_{ac}} N_p \sigma_0 \tau_{eff} . \tag{2.92}$$

2.10 Slope Efficiency

Slope efficiency is the change in output power with current, $\frac{dP}{dI}$. From our rate equations, we have something close to power and current; we have terms of photon flux ϕ_{ph} and current density J. We can therefore solve for $\frac{d\phi_{ph}}{dJ}$ and convert to slope efficiency

$$\underset{\text{efficiency}}{\text{slope}} = \underset{in}{change}\left(\frac{\text{number of cavity photons}}{\text{pump current}}\right) \times \underset{\text{energy}}{\text{photon}} \times \underset{\text{escape rate}}{\text{photon}}$$

so

$$\frac{dP}{dI} = \frac{d\phi_{ph}}{dJ}\frac{\frac{V_m}{v_g}}{A} \times \mathcal{E}_{ph} \times \frac{1}{\tau_m}\,. \tag{2.93}$$

where the photon escape rate $\frac{1}{\tau_m}$ is

$$\frac{1}{\tau_m} = v_g \alpha_m\,. \tag{2.94}$$

To simplify the analysis, we will first look at the case of identical QC periods (*i.e.* all $\bar{U}_i = 1$ and all $n_{u,i}$ and $n_{\ell,i}$ are the same). To solve for $\phi_{ph}(J)$, we can start by solving for the steady state condition of Eq. (2.79c), $\frac{d\phi_{ph}}{dt} = 0$:

$$n_u - n_\ell = \frac{L_{ph}}{\tau_{ph} v_g \sigma_0 N_p}\,. \tag{2.95}$$

To find a relation for $n_u - n_\ell$, we solve the steady state conditions of Eqs. (2.79a) and (2.79b), and recover for n_u and n_ℓ, respectively,

$$n_u = \eta_{inj}\frac{J}{q}\frac{\frac{1}{\tau_\ell} + \sigma_0\phi_{ph}}{\frac{1}{\tau_u}\frac{1}{\tau_\ell} + \sigma_0\phi_{ph}\left(\frac{1}{\tau_u} + \frac{1}{\tau_\ell} - \frac{1}{\tau_{u\ell}}\right)} \tag{2.96a}$$

$$n_\ell = \eta_{inj}\frac{J}{q}\frac{\frac{1}{\tau_{u\ell}} + \sigma_0\phi_{ph}}{\frac{1}{\tau_u}\frac{1}{\tau_\ell} + \sigma_0\phi_{ph}\left(\frac{1}{\tau_u} + \frac{1}{\tau_\ell} - \frac{1}{\tau_{u\ell}}\right)} \tag{2.96b}$$

so that combining Eq. (2.96a) and Eq. (2.96b) yields

$$n_u - n_\ell = \eta_{inj}\frac{J}{q}\frac{\tau_u\left(1 - \frac{\tau_\ell}{\tau_{u\ell}}\right)}{1 + \sigma_0\phi_{ph}\left(\tau_u\left(1 - \frac{\tau_\ell}{\tau_{u\ell}}\right) + \tau_\ell\right)} = \eta_{inj}\frac{J}{q}\frac{\tau_{eff}}{1 + \sigma_0\phi_{ph}\left(\tau_{eff} + \tau_\ell\right)} \tag{2.97}$$

using $\tau_{eff} = \tau_u\left(1 - \frac{\tau_\ell}{\tau_{u\ell}}\right)$. Combining the results of Eqs. (2.95) and (2.97) gives

$$\phi_{ph} = \eta_{inj}\frac{J}{q}\frac{\tau_{ph}v_g N_p}{L_p}\frac{\tau_{eff}}{\left(\tau_{eff}+\tau_\ell\right)} - \frac{1}{\sigma_0\left(\tau_{eff}+\tau_\ell\right)} \tag{2.98}$$

and

$$\frac{d\phi_{ph}}{dJ} = \eta_{inj}\frac{v_g N_p \tau_{ph}}{qL_p}\frac{\tau_{eff}}{\left(\tau_{eff}+\tau_\ell\right)}\,. \tag{2.99}$$

Plugging Eq. (2.99) into Eq. (2.93), we get that the slope efficiency is

$$\frac{dP}{dI} = \eta_{inj}N_p\frac{\mathcal{E}_{ph}}{q}\frac{\alpha_m}{\alpha_m+\alpha_w}\frac{\tau_{eff}}{\left(\tau_{eff}+\tau_\ell\right)} \tag{2.100}$$

where the cavity escape and photon lifetimes have been converted to the more common mirror and waveguide loss terms. Finally, the inclusion of the local field intensity $\bar{U}_i$ adds a "modal efficiency" factor η_m given by [54]

$$\eta_m = \frac{\left(\sum_{i=1}^{N_p}\bar{U}_i\right)^2}{N_p\sum_{i=1}^{N_p}\bar{U}_i^2} \tag{2.101}$$

and so

$$\frac{dP}{dI} = \eta_{inj}\eta_m N_p\frac{\mathcal{E}_{ph}}{q}\frac{\alpha_m}{\alpha_m+\alpha_w}\frac{\tau_{eff}}{\left(\tau_{eff}+\tau_\ell\right)}\,. \tag{2.102}$$

2.11 Output Power and Wall-plug Efficiency

Having solved for the slope efficiency, a linear relationship for output power results for currents above threshold.

$$P = \frac{dP}{dI}(I - I_{th}) = N_p\frac{\mathcal{E}_{ph}}{q}\frac{\alpha_m}{\alpha_m+\alpha_w}\frac{\tau_{eff}}{\left(\tau_{eff}+\tau_\ell\right)}\eta_{inj}\eta_m(I - I_{th}) \tag{2.103}$$

Wall-plug efficiency is simply defined as power out for power in. The input power is simply voltage times current, where the voltage can be broken up into the component terms representing the photon energy drop $\mathcal{E}_{ph}$, the energy drop Δ_{inj} from the lower laser state of one active region to the upper laser state of the adjacent down-stream active region, and any parasitic series resistance IR_{series}. Thus, input power P_{in} is given

by

$$P_{in} = \left(\frac{N_p}{q} (\mathcal{E}_{ph} + \Delta_{inj}) + IR_{series} \right) I \tag{2.104}$$

and the wall-plug efficiency η_{wp} is

$$\eta_{wp} = \left(\frac{\mathcal{E}_{ph}}{\mathcal{E}_{ph} + \Delta_{inj} + \frac{IR_{series}}{N_p}} \right) \left(\frac{\tau_{eff}}{\tau_{eff} + \tau_\ell} \right) \left(\frac{\alpha_m}{\alpha_m + \alpha_w} \right) \left(\frac{J - J_{th}}{J} \right) \eta_{inj} \eta_m \tag{2.105}$$

expressed as a product of constituent terms, each representing a source of efficiency loss.

2.12 Maximum Current & Differential Resistance

It is often useful to conceptualize transport through a QC structure in terms of total, aggregate transit time τ_{trans} through a single QC period. The velocity of electron flow v_{trans} is thus simply given as,

$$v_{trans} = \frac{L_p}{\tau_{trans}} \,. \tag{2.106}$$

This transport velocity can be used as a fundamental component of current density J, which also multiplies the electron density participating in transport N_{trans} $[\frac{1}{\text{volume}}]$ [55].

$$J = qN_{trans}v_{trans} \tag{2.107}$$

With substitution of Eq. (2.106), Eq. (2.107) becomes

$$J = \frac{qn_{trans}}{\tau_{trans}} \tag{2.108}$$

where $n_{trans} = \frac{N_{trans}}{L_p}$ $[\frac{1}{\text{area}}]$ is the sheet density of electrons participating in transport. The total sheet density of electrons present in the system n_s is assumed, for a QC structure, to be the doping density (typically, $n_s \sim 10^{11}$ cm^{-2}). We can now distinguish between those electrons participating in transport n_{trans} and those doped electrons that are otherwise "trapped" or stationary in the structure $n_{stationary}$, so that

$$n_s = n_{trans} + n_{stationary} \,. \tag{2.109}$$

When all system electrons are participating in current transport, so that $n_s = n_{trans}$ and $n_{stationary} = 0$, we achieve maximum current density J_{max}.

$$J_{max} = \frac{q n_s}{\tau_{trans}} \tag{2.110}$$

The linear relationship of J_{max} and n_s has been confirmed for QC devices [56] [57].

Since current transport can be conceptually understood through electron transit time, it is also useful to relate device resistance R (more accurately, differential resistance $\frac{dV}{dI}$) in a similar way. Here, we use simple, classical semiconductor device physics (see [55], for example) to first relate conductivity σ as

$$\sigma = q \frac{v_{trans}}{E_{field}} N_{trans} \tag{2.111}$$

where the mobility is given by $\frac{v_{trans}}{E_{field}}$. Now, resistance is simply

$$R = \frac{1}{\sigma} \frac{N_p L_p}{A} \tag{2.112}$$

so combining with Eqs. (2.106) and (2.111),

$$R = \frac{E_{field}}{q N_{trans}} \frac{N_p \tau_{trans}}{A} . \tag{2.113}$$

Taking E_{field} in terms of the applied voltage V_{appl} so that

$$E_{field} = \frac{V_{appl}}{N_p L_p} \tag{2.114}$$

we realize our relation for resistance and transit time.

$$R = \frac{V_{appl}}{q A} \frac{\tau_{trans}}{n_{trans}} \tag{2.115}$$

where $n_{trans} = L_p N_{trans}$. From our relations for J_{max} and R, we can visualize the transit rate $\frac{1}{\tau_{trans}}$ as the size of the "pipe" through which electrons can flow. The bigger the pipe (*i.e.* the shorter τ_{trans}), the more electrons one can send through the structure and therefore the more electrons are available to produce photons.

2.13 Summary

In this chapter, I have provided a comprehensive toolbox of derivations, equations, and relations of fundamental importance to QC laser operation. At times, the ability to understand from basic principles the origin of a laser parameter, threshold current for example, can help to innovate strategies to improve that parameter. This chapter provides such understanding. We have also now established a basis for understanding the new design strategies and interpretation of unique observed data presented in subsequent chapters.

References

[1] D. M. Chapin, C. S. Fuller, and G. L. Pearson, "A New Silicon p-n Junction Photocell for Converting Solar Radiation into Electrical Power," *J. Appl. Phys.* **25**, 676 (1954). doi:10.1063/1.1721711

[2] R. N. Hall, G. E. Fenner, J. D. Kingsley, T. J. Soltys, and R. O. Carlson, "Coherent Light Emission From GaAs Junctions," *Phys. Rev. Lett.* **9**, 366 (1962). doi:10.1103/PhysRevLett.9.366

[3] J. Nick Holonyak and S. F. Bevacqua, "Coherent (Visible) Light Emission from $Ga(As_{1-x}P_x)$ Junctions," *Appl. Phys. Lett.* **1**, 82 (1962). doi:10.1063/1.1753706

[4] Z. I. Alferov, "The double heterostructure concept and its applications in physics, electronics, and technology," *Rev. Mod. Phys.* **73**, 767 (2001). doi:10.1103/RevModPhys.73.767

[5] H. Kroemer, "Quasielectric fields and band offsets: teaching electrons new tricks," *Rev. Mod. Phys.* **73**, 783 (2001). doi:10.1103/RevModPhys.73.783

[6] L. Esaki and R. Tsu, "Superlattice and Negative Differential Conductivity in Semiconductors," *IBM J. Res. Dev.* **14**, 61 (1970). url: http://www.research.ibm.com/journal/rd/141/ibmrd1401H.pdf

[7] R. F. Kazarinov and R. A. Suris, "Possibility of Amplification of Electromagnetic Waves in a Semiconductor with a Superlattice," *Sov. Phys. Semicond.* **5**, 207 (1971).

[8] J. Faist, F. Capasso, D. L. Sivco, C. Sirtori, A. L. Hutchinson, and A. Y. Cho, "Quantum Cascade Laser," *Science* **264**, 553 (1994). doi:10.1126/science.264.5158.553

[9] B. S. Williams, "Terahertz quantum-cascade lasers," *Nature Photonics* **1**, 517 (2007).
doi:10.1038/nphoton.2007.166

[10] J. Devenson, O. Cathabard, R. Teissier, and A. N. Baranov, "InAs/AlSb quantum cascade lasers emitting at 2.75–2.97 µm," *Appl. Phys. Lett.* **91**, 251102 (2007).
doi:10.1063/1.2825284

[11] R. Colombelli, F. Capasso, C. Gmachl, A. L. Hutchinson, D. L. Sivco, A. Tredicucci, M. C. Wanke, A. M. Sergent, and A. Y. Cho, "Far-infrared surface–plasmon quantum–cascade lasers at 21.5 µm and 24 µm wavelengths," *Appl. Phys. Lett.* **78**, 2620 (2001).
doi:10.1063/1.1367304

[12] Senior Airman Julianne Showalter, *United States Air Force*

[13] BAE Systems, "BAE SYSTEMS' ATIRCM/CMWS Successfully Completes Army Live-fire Tests; Key Testing Milestone Accomplished," *Press Release* (May 15, 2001).

[14] H. Manor and S. Arnon, "Performance of an Optical Wireless Communication System as a Function of Wavelength," *Appl. Opt.* **42**, 4285 (2003).
doi:10.1364/AO.42.004285

[15] A. A. Kosterev, R. F. Curl, F. K. Tittel, M. Rochat, D. Hofstetter, and J. Faist, "Chemical sensing with pulsed QC–DFB lasers operating at 15.6 µm," *Appl. Phys. B* **75**, 351 (2002).
doi:10.1007/s00340-002-0963-z

[16] M. Beck, D. Hofstetter, T. Aellen, J. Faist, U. Oesterle, M. Ilegems, E. Gini, and H. Melchior, "Continuous Wave Operation of a Mid-Infrared Semiconductor Laser at Room Temperature," *Science* **295**, 301 (2002).
doi:10.1126/science.1066408

[17] G. Scamarcio, F. Capasso, C. Sirtori, J. Faist, A. L. Hutchinson, D. L. Sivco, and A. Y. Cho, "High-Power Infrared (8-Micrometer Wavelength) Superlattice Lasers,"

Science **276**, 773 (1997).
doi:10.1126/science.276.5313.773

[18] M. Troccoli, A. Belyanin, F. Capasso, E. Cubukcu, D. L. Sivco, and A. Y. Cho, "Raman injection laser," *Nature* **433**, 845 (2005).
doi:10.1038/nature03330

[19] R. Terazzi, T. Gresch, M. Giovannini, N. Hoyler, N. Sekine, and J. Faist, "Bloch gain in quantum cascade lasers," *Nature Physics* **3**, 329 (2007).
doi:10.1038/nphys577

[20] K.-Y. Cheng, "Molecular beam epitaxy technology of III–V compound semiconductors for optoelectronic applications," *Proc. IEEE* **85**, 1694 (1997).
doi:10.1109/5.649646

[21] J. Coleman, "Metalorganic chemical vapor deposition for optoelectronic devices," *Proc. IEEE* **85**, 1715 (1997).
doi:10.1109/5.649647

[22] Z. Liu, D. Wasserman, S. Howard, A. Hoffman, C. Gmachl, X. Wang, T. Tanbun-Ek, L. Cheng, and F.-S. Choa, "Room-temperature continuous-wave quantum cascade lasers grown by MOCVD without lateral regrowth," **18**, 1347 (2006).
doi:10.1109/LPT.2006.877006

[23] M. Razeghi, "High-power high-wall plug efficiency mid-infrared quantum cascade lasers based on InP/GaInAs/InAlAs material system," *Proc. SPIE* **7230**, 723011 (2009).
doi:10.1117/12.813923

[24] K. J. Franz, W. O. Charles, A. Shen, A. J. Hoffman, M. C. Tamargo, and C. Gmachl, "ZnCdSe/ZnCdMgSe quantum cascade electroluminescence," *Appl. Phys. Lett.* **92**, 121105 (2008).
doi:10.1063/1.2903135

[25] K. J. Franz, D. Wasserman, A. J. Hoffman, D. C. Jangraw, K.-T. Shiu, S. R. Forrest, and C. Gmachl, "Evidence of cascaded emission in a dual-wavelength quantum

cascade laser," *Appl. Phys. Lett.* **90**, 091104 (2007).
doi:10.1063/1.2709970

[26] K. J. Franz, S. Menzel, A. J. Hoffman, D. Wasserman, J. W. Cockburn, and C. Gmachl, "High *k*-space lasing in a dual-wavelength quantum cascade laser," *Nature Photonics* **3**, 50 (2008).
doi:10.1038/nphoton.2008.250

[27] C. Sirtori, F. Capasso, J. Faist, and S. Scandolo, "Nonparabolicity and a sum rule associated with bound-to-bound and bound-to-continuum intersubband transitions in quantum wells," *Phys. Rev. B* **50**, 8663 (1994).
doi:10.1103/PhysRevB.50.8663

[28] P. Harrison, *Quantum Wells, Wires and Dots: Theoretical and Computational Physics of Semiconductor Nanostructures* Wiley 2nd edn. (2005).
ISBN 0-470-01080-0

[29] I. Vurgaftman, J. R. Meyer, and L. R. Ram-Mohan, "Band parameters for III–V compound semiconductors and their alloys," *J. Appl. Phys.* **89**, 5815 (2001).
doi:10.1063/1.1368156

[30] G. Dehlinger, L. Diehl, U. Gennser, H. Sigg, J. Faist, K. Ensslin, D. Grutzmacher, and E. Muller, "Intersubband Electroluminescence from Silicon-Based Quantum Cascade Structures," *Science* **290**, 2277 (2000).
doi:10.1126/science.290.5500.2277

[31] O. Malis, L. N. Pfeiffer, K. W. West, A. M. Sergent, and C. Gmachl, "Mid-infrared hole-intersubband electroluminescence in carbon-doped GaAs/AlGaAs quantum cascade structures," *Appl. Phys. Lett.* **88**, 081117 (2006).
doi:10.1063/1.2179117

[32] S. Adachi, *Properties of Group-IV, III-V and II-VI Semiconductors* Wiley (2005).
ISBN 0-470-09032-4

[33] Y. P. Varshni, "Temperature dependence of the energy gap in semiconductors," *Physica* **34**, 149 (1967).
doi:10.1016/0031-8914(67)90062-6

[34] J. Faist, F. Capasso, D. L. Sivco, A. L. Hutchinson, S.-N. G. Chu, and A. Y. Cho, "Short wavelength ($\lambda \sim 3.4$ μm) quantum cascade laser based on strained compensated InGaAs/AlInAs," *Appl. Phys. Lett.* **72**, 680 (1998).
doi:10.1063/1.120843

[35] S. L. Chuang, *Physics of Optoelectronic Devices* Wiley, New York (1995).
ISBN 0-471-10939-8

[36] G. L. Bir and G. Pikus, *Symmetry and Strain-Induced Effects in Semiconductors* Wiley, New York (1974).
ISBN 0-470-07321-7

[37] C. G. Van de Walle, "Band lineups and deformation potentials in the model-solid theory," *Phys. Rev. B* **39**, 1871 (1989).
doi:10.1103/PhysRevB.39.1871

[38] M. Sugawara, N. Okazaki, T. Fujii, and S. Yamazaki, "Conduction-band and valence-band structures in strained $In_{1-x}Ga_xAs$/InP quantum wells on (001) InP substrates," *Phys. Rev. B* **48**, 8102 (1993).
doi:10.1103/PhysRevB.48.8102

[39] D. F. Nelson, R. C. Miller, and D. A. Kleinman, "Band nonparabolicity effects in semiconductor quantum wells," *Phys. Rev. B* **35**, 7770 (1987).
doi:10.1103/PhysRevB.35.7770

[40] J. H. Davies, *The Physics of Low-Dimensional Semiconductors* Cambridge Univ. Press (1998).
ISBN 0-521-48491-X

[41] C. Cohen-Tannoudji, B. Diu, and F. Laloë, *Quantum Mechanics* Wiley (1977).
ISBN 0-471-16433-X

[42] A. Yariv, *Quantum Electronics* Wiley, New York 2nd edn. (1989).
ISBN 0-471-60997-8

[43] M. A. Parker, *Physics of Optoelectronics* Taylor & Francis (2005).
ISBN 0-8247-5385-2

[44] J. H. Smet, C. G. Fonstad, and Q. Hu, "Intrawell and interwell intersubband transitions in multiple quantum wells for far-infrared sources," *J. Appl. Phys.* **79**, 9305 (1996).
doi:10.1063/1.362607

[45] B. E. A. Saleh and M. C. Teich, *Fundamentals of Photonics* Wiley (1991).
ISBN 0-471-83965-5

[46] E. Rosencher and B. Vinter, *Optoelectronics* Cambridge Univ. Press (2002).
ISBN 0-521-77129-3

[47] G. Bastard, *Wave Mechanics Applied to Semiconductor Heterostructures* Wiley (1991).
ISBN 0-470-21708-1

[48] R. P. Leavitt, "Empirical two-band model for quantum wells and superlattices in an electric field," *Phys. Rev. B* **44**, 11270 (1991).
doi:10.1103/PhysRevB.44.11270

[49] A. E. Siegman, *Lasers* Univ. Science Books (1986).
ISBN 0935702113

[50] R. Ferreira and G. Bastard, "Evaluation of some scattering times for electrons in unbiased and biased single- and multiple-quantum-well structures," *Phys. Rev. B* **40**, 1074 (1989).
doi:10.1103/PhysRevB.40.1074

[51] C. Gmachl, D. L. Sivco, R. Colombelli, F. Capasso, and A. Y. Cho, "Ultra-broadband semiconductor laser," *Nature* **415**, 883 (2002).
doi:10.1038/415883a

[52] A. J. Hoffman, S. Schartner, S. S. Howard, K. J. Franz, F. Towner, and C. Gmachl, "Low voltage-defect quantum cascade laser with heterogeneous injector regions," *Opt. Express* **15**, 15818 (2007).
doi:10.1364/OE.15.015818

[53] L. A. Coldren and S. W. Corzine, *Diode Lasers and Photonic Integrated Circuits* Wiley, New York (1995).
ISBN 0-471-11875-3

[54] T. Gresch, M. Giovannini, N. Hoyer, and J. Faist, "Quantum cascade lasers with large optical waveguides," **18**, 544 (2006).
doi:10.1109/LPT.2005.863633

[55] S. M. Sze, *Physics of Semiconductor Devices* Wiley 2nd edn. (1981).
ISBN 0-471-05661-8

[56] T. Aellen, M. Beck, N. Hoyler, M. Giovannini, J. Faist, and E. Gini, "Doping in quantum cascade lasers. I. InAlAs–InGaAs/InP midinfrared devices," *J. Appl. Phys.* **100**, 043101 (2006).
doi:10.1063/1.2234804

[57] S. S. Howard, D. P. Howard, K. Franz, A. Hoffman, D. L. Sivco, and C. F. Gmachl, "The effect of injector barrier thickness and doping level on current transport and optical transition width in a $\lambda \sim 8.0$ μm quantum cascade structure," *Appl. Phys. Lett.* **93**, 191107 (2008).
doi:10.1063/1.3028013

[58] L. Shterengas, G. Belenky, T. Hosoda, G. Kipshidze, and S. Suchalkin, "Continuous wave operation of diode lasers at 3.36 μm at 12 °C," *Appl. Phys. Lett.* **93**, 011103 (2008).
doi:10.1063/1.2953210

[59] J. S. Yu, A. Evans, S. Slivken, S. R. Darvish, and M. Razeghi, "Temperature dependent characteristics of $\lambda \sim 3.8$ μm room-temperature continuous-wave quantum-cascade lasers," *Appl. Phys. Lett.* **88**, 251118 (2006).
doi:10.1063/1.2216024

[60] R. Q. Yang, B. H. Yang, D. Zhang, C.-H. Lin, S. J. Murry, H. Wu, and S. S. Pei, "High power mid-infrared interband cascade lasers based on type–II quantum wells," *Appl. Phys. Lett.* **71**, 2409 (1997).
doi:10.1063/1.120076

[61] M. Kim, C. L. Canedy, W. W. Bewley, C. S. Kim, J. R. Lindle, J. Abell, I. Vurgaftman, and J. R. Meyer, "Interband cascade laser emitting at λ = 3.75 μm in continuous wave above room temperature," *Appl. Phys. Lett.* **92**, 191110 (2008). doi:10.1063/1.2930685

[62] S. Forouhar and K. Mansour, *private communication* (2008).

[63] Y. Bai, S. Slivken, S. R. Darvish, and M. Razeghi, "Room temperature continuous wave operation of quantum cascade lasers with 12.5% wall plug efficiency," *Appl. Phys. Lett.* **93** (2008). doi:10.1063/1.2957673

[64] L. Wilson, J. Cockburn, D. Carder, M. Steer, M. Hopkinson, C. Chia, R. Airey, and G. Hill, "λ = 8.3 μm GaAs/AlAs quantum cascade lasers incorporating InAs monolayers," *Electron. Lett.* **37**, 1292 (2001). doi:10.1049/el:20010865

[65] Q. Yang, C. Mann, F. Fuchs, K. Köhler, and W. Bronner, "High-temperature ($T \geq$ 400 K) operation of strain-compensated quantum cascade lasers with thin InAs insertion layers and AlAs blocking barriers," *J. Cryst. Growth* **278**, 714 (2005). doi:10.1016/j.jcrysgro.2005.01.001

[66] A. Friedrich, G. Boehm, and M. C. Amann, "Short-wavelength intersubband staircase lasers, with and without AlAs-blocking barriers," *Semicond. Sci. Technol.* **22**, 218 (2007). doi:10.1088/0268-1242/22/3/008

[67] D. G. Revin, M. R. Soulby, J. W. Cockburn, Q. Yang, C. Manz, and J. Wagner, "Dispersive gain and loss in midinfrared quantum cascade laser," *Appl. Phys. Lett.* **92**, 081110 (2008). doi:10.1063/1.2884699

[68] M. P. Semtsiv, M. Ziegler, S. Dressler, W. T. Masselink, N. Georgiev, T. Dekorsy, and M. Helm, "Above room temperature operation of short wavelength (λ = 3.8 μm) strain-compensated $In_{0.73}Ga_{0.27}As$–AlAs quantum-cascade lasers," *Applied Physics Letters* **85**, 1478 (2004). doi:10.1063/1.1789246

[69] R. Teissier, J. J. Finley, M. S. Skolnick, J. W. Cockburn, J. L. Pelouard, R. Grey, G. Hill, M. A. Pate, and R. Planel, "Experimental determination of Γ–X intervalley transfer mechanisms in GaAs/AlAs heterostructures," *Phys. Rev. B* **54**, R8329 (1996). doi:10.1103/PhysRevB.54.R8329

[70] M. P. Semtsiv, M. Wienold, S. Dressler, W. T. Masselink, G. Fedorov, and D. Smirnov, "Intervalley carrier transfer in short-wavelength InP-based quantum-cascade laser," *Appl. Phys. Lett.* **93**, 071109 (2008). doi:10.1063/1.2973212

[71] C. Gmachl, H. M. Ng, and A. Y. Cho, "Intersubband absorption in GaN/AlGaN multiple quantum wells in the wavelength range of $\lambda \sim$ 1.75-4.2 μm," *Appl. Phys. Lett.* **77**, 334 (2000). doi:10.1063/1.126968

[72] L. Nevou, M. Tchernycheva, F. H. Julien, F. Guillot, and E. Monroy, "Short wavelength ($\lambda = 2.13$ μm) intersubband luminescence from GaN/AlN quantum wells at room temperature," *Appl. Phys. Lett.* **90**, 121106 (2007). doi:10.1063/1.2715001

[73] A. Vardi, G. Bahir, F. Guillot, C. Bougerol, E. Monroy, S. E. Schacham, M. Tchernycheva, and F. H. Julien, "Near infrared quantum cascade detector in GaN/AlGaN/AlN heterostructures," *Appl. Phys. Lett.* **92**, 011112 (2008). doi:10.1063/1.2830704

[74] K. Jinen, T. Kikuchi, M. Watanabe, and M. Asada, "Room-temperature electroluminescence from single-period (CdF_2/CaF_2) inter-subband quantum cascade structure on Si substrate," *Jap. J. Appl. Phys.* **45**, 3656 (2006). doi:10.1143/JJAP.45.3656

[75] S. Nakamura, M. Senoh, S. ichi Nagahama, N. Iwasa, T. Yamada, T. Matsushita, H. Kiyoku, and Y. Sugimoto, "InGaN-Based Multi-Quantum-Well-Structure Laser Diodes," *Jap. J. Appl. Phys.* **35**, L74 (1996). doi:10.1143/JJAP.35.L74

[76] S. Guo and M. C. Tamargo, "II–VI Materials for Visible Light Emitters," in "II–VI Semiconductor Materials and their Applications," (edited by M. C. Tamargo) vol. 12 of *Optoelectronic Properties of Semiconductors and Superlattices* Taylor & Francis (2002).
ISBN 1560329149

[77] M. Tamargo, A. Cavus, L. Zeng, N. Dai, N. Bambha, A. Gray, F. Semendy, W. Krystek, and F. Pollak, "MBE growth of lattice–matched ZnCdMgSe quaternaries and ZnCdMgSe/ZnCdSe quantum wells on InP substrates," *J. Electron. Mater.* **25**, 259 (1996).
doi:10.1007/BF02666254

[78] Y. Guo, G. Aizin, Y. C. Chen, L. Zeng, A. Cavus, and M. C. Tamargo, "Photo-pumped ZnCdSe/ZnCdMgSe blue-green quantum well lasers grown on InP substrates," *Appl. Phys. Lett.* **70**, 1351 (1997).
doi:10.1063/1.118576

[79] DARPA MTO, "Broad Agency Announcment for the DARPA Visible InGaN Injection Lasers (VIGIL) program."
url: http://www.darpa.mil/mto/solicitations/baa07-28/pdf/VIGIL.pdf

[80] J. R. Chelikowsky and M. L. Cohen, "Nonlocal pseudopotential calculations for the electronic structure of eleven diamond and zinc-blende semiconductors," *Phys. Rev. B* **14**, 556 (1976).
doi:10.1103/PhysRevB.14.556

[81] O. Zakharov, A. Rubio, X. Blase, M. L. Cohen, and S. G. Louie, "Quasiparticle band structures of six II–VI compounds: ZnS, ZnSe, ZnTe, CdS, CdSe, and CdTe," *Phys. Rev. B* **50**, 10780 (1994).
doi:10.1103/PhysRevB.50.10780

[82] M. Sohel, M. Muñoz, and M. C. Tamargo, "Molecular beam epitaxial growth and characterization of zinc–blende ZnMgSe on InP (001)," *Appl. Phys. Lett.* **85**, 2794 (2004).
doi:10.1063/1.1804611

[83] M. J. Kastner, B. Hahn, C. Auchter, M. Deufel, A. Rosenauer, and W. Gebhardt, "Structural characterization and MOVPE growth of ZnCdSe and ZnSSe layers, quantum wells and superlattices," *J. Cryst. Growth* **159**, 134 (1996). doi:10.1016/0022-0248(95)00761-X

[84] M. A. Haase, J. Qiu, J. M. DePuydt, and H. Cheng, "Blue–green laser diodes," *Appl. Phys. Lett.* **59**, 1272 (1991). doi:10.1063/1.105472

[85] N. Dai, A. Cavus, R. Dzakpasu, M. C. Tamargo, F. Semendy, N. Bambha, D. M. Hwang, and C. Y. Chen, "Molecular beam epitaxial growth of high quality $Zn_{1-x}Cd_xSe$ on InP substrates," *Appl. Phys. Lett.* **66**, 2742 (1995). doi:10.1063/1.113694

[86] M. T. Litz, K. Watanabe, M. Korn, H. Ress, U. Lunz, W. Ossau, A. Waag, G. Landwehr, T. Walter, B. Neubauer, D. Gerthsen, and U. Schüssler, "Epitaxy of $Zn_{1-x}Mg_xSe_yTe_{1-y}$ on (100)InAs," *J. Cryst. Growth* **159**, 54 (1996). doi:10.1016/0022-0248(95)00881-0

[87] L. Zeng, B. X. Yang, M. C. Tamargo, E. Snoeks, and L. Zhao, "Quality improvements of $Zn_xCd_yMg_{1-x-y}Se$ layers grown on InP substrates by a thin ZnCdSe interfacial layer," *Appl. Phys. Lett.* **72**, 1317 (1998). doi:10.1063/1.120980

[88] D. Li and M. D. Pashley, "ZnSe nucleation on the GaAs(001):Se-(2×1) surface observed by scanning tunneling microscopy," *J. Vac. Sci. Tech. B* **12**, 2547 (1994). doi:10.1116/1.587799

[89] L. Zeng, S. P. Guo, Y. Y. Luo, W. Lin, M. C. Tamargo, H. Xing, and G. S. Cargill, "Defect reduction of $Zn_xCd_yMg_{1-x-y}Se$ based structures grown on InP by using Zn irradiation of the III–V surface," *J. Vac. Sci. Tech. B* **17**, 1255 (1999). doi:10.1116/1.590734

[90] B. S. Li, A. Shen, W. O. Charles, Q. Zhang, and M. C. Tamargo, "Midinfrared intersubband absorption in wide band gap II–VI $Zn_xCd_{1-x}Se$ multiple quantum wells with metastable zincblende MgSe barriers," *Appl. Phys. Lett.* **92**, 261104

(2008).
doi:10.1063/1.2943660

[91] H. Lu, A. Shen, W. Charles, I. Yokomizo, M. C. Tamargo, K. J. Franz, C. Gmachl, and M. Muñoz, "Optical characterization of intersubband transitions in $Zn_xCd_{1-x}Se/Zn_{x'}Cd_{y'}Mg_{1-x'-y'}Se$ multiple quantum well structures by contactless electroreflectance," *Appl. Phys. Lett.* **89**, 241921 (2006).
doi:10.1063/1.2405385

[92] D. Walsh, K. Mazuruk, and M. Benzaquen, "Raman spectrum of a ZnSe/GaAs heterostructure," *Phys. Rev. B* **36**, 2883 (1987).
doi:10.1103/PhysRevB.36.2883

[93] P. Y. Yu, "Resonant Raman study of the LO + acoustic phonon modes in CdSe," *Solid State Comm.* **19**, 1087 (1976).
doi:10.1016/0038-1098(76)90104-6

[94] M. Muñoz, H. Lu, X. Zhou, M. C. Tamargo, and F. H. Pollak, "Band offset determination of $Zn_{0.53}Cd_{0.47}Se/Zn_{0.29}Cd_{0.24}Mg_{0.47}Se$," *Appl. Phys. Lett.* **83**, 1995 (2003).
doi:10.1063/1.1606875

[95] T. Miyajima, H. Okuyama, and K. Akimoto, "Ti/Pt/Au Ohmic Contacts to n-Type ZnSe," *Jap. J. Appl. Phys.* **31**, L1743 (1992).
doi:10.1143/JJAP.31.L1743

[96] J. Faist, F. Capasso, C. Sirtori, D. L. Sivco, A. L. Hutchinson, and A. Y. Cho, "Vertical transition quantum cascade laser with Bragg confined excited state," *Appl. Phys. Lett.* **66**, 538 (1995).
doi:10.1063/1.114005

[97] V. Moreau, M. Bahriz, R. Colombelli, R. Perahia, O. Painter, L. R. Wilson, and A. B. Krysa, "Demonstration of air-guided quantum cascade lasers without top claddings," *Opt. Express* **15**, 14861 (2007).
doi:10.1364/OE.15.014861

[98] V. R. Almeida, Q. Xu, C. A. Barrios, and M. Lipson, "Guiding and confining light in void nanostructure," *Opt. Lett.* **29**, 1209 (2004).
doi:10.1364/OL.29.001209

[99] United States Nuclear Regulatory Comission, "Uranium Enrichment."
url: http://www.nrc.gov/materials/fuel-cycle-fac/ur-enrichment.html

[100] P. Rabinowitz, A. Kaldor, A. Gnauck, R. L. Woodin, and J. S. Gethner, "Two-color infrared isotopically selective decomposition of UF_6," *Opt. Lett.* **7**, 212 (1982).
doi:10.1364/OL.7.000212

[101] Y. Okada, S. Tanimura, H. Okamura, A. Suda, H. Tashiro, and K. Takeuchi, "Vibrational spectroscopy and predissociation of UF_6 clusters in a supersonic Laval nozzle," *J. Molec. Struct.* **410-411**, 299 (1997).
doi:10.1016/S0022-2860(96)09567-1

[102] C. Gmachl, F. Capasso, A. Tredicucci, D. Sivco, A. Hutchinson, and A. Cho, "Long wavelength $\lambda \simeq 13\,\mu$m quantum cascade lasers," *Electron. Lett.* **34**, 1103 (1998).
url: http://ieeexplore.ieee.org/xpls/abs_all.jsp?arnumber=684577

[103] A. Tredicucci, C. Gmachl, F. Capasso, D. L. Sivco, A. L. Hutchinson, and A. Y. Cho, "Long wavelength superlattice quantum cascade lasers at $\lambda \simeq 17\,\mu$m," *Appl. Phys. Lett.* **74**, 638 (1999).
doi:10.1063/1.123026

[104] A. Tredicucci, C. Gmachl, M. C. Wanke, F. Capasso, A. L. Hutchinson, D. L. Sivco, S. G. Chu, and A. Y. Cho, "Surface plasmon quantum cascade lasers at $\lambda \sim 19\,\mu$m," *Appl. Phys. Lett.* **77**, 2286 (2000).
doi:10.1063/1.1316768

[105] M. Rochat, D. Hofstetter, M. Beck, and J. Faist, "Long–wavelength ($\lambda \approx 16\,\mu$m), room–temperature, single–frequency quantum–cascade lasers based on a bound–to–continuum transition," *Appl. Phys. Lett.* **79**, 4271 (2001).
doi:10.1063/1.1425468

[106] S. Tsujino, A. Borak, E. Müller, M. Scheinert, C. V. Falub, H. Sigg, D. Grützmacher, M. Giovannini, and J. Faist, "Interface–roughness–induced broadening of intersubband electroluminescence in p-SiGe and n-GaInAs/AlInAs quantum-cascade structures," *Appl. Phys. Lett.* **86**, 062113 (2005).
doi:10.1063/1.1862344

[107] M. O. Scully and M. S. Zubairy, *Quantum Optics* Cambridge Univ. Press, New York (1997).
ISBN 0-521-43595-1

[108] G. Scalari, C. Walther, J. Faist, H. Beere, and D. Ritchie, "Electrically switchable, two-color quantum cascade laser emitting at 1.39 and 2.3 THz," *Appl. Phys. Lett.* **88**, 141102 (2006).
doi:10.1063/1.2191407

[109] C. Sirtori, A. Tredicucci, F. Capasso, J. Faist, D. L. Sivco, A. L. Hutchinson, and A. Y. Cho, "Dual–wavelength emission from optically cascaded intersubband transitions," *Opt. Lett.* **23**, 463 (1998).
doi:10.1364/OL.23.000463

[110] S. S. Howard, Z. Liu, and C. F. Gmachl, "Thermal and stark-effect roll-over of quantum-cascade lasers," *IEEE J. Quantum Electron.* **44**, 319 (2008).
doi:10.1109/JQE.2007.912477

[111] J. Faist, F. Capasso, C. Sirtori, D. L. Sivco, A. L. Hutchinson, M. S. Hybertsen, and A. Y. Cho, "Quantum Cascade Lasers without Intersubband Population Inversion," *Phys. Rev. Lett.* **76**, 411 (1996).
doi:10.1103/PhysRevLett.76.411

[112] G. B. Serapiglia, K. L. Vodopyanov, and C. C. Phillips, "Nonequilibrium electron distributions in a three-subband InGaAs/InAlAs quantum well studied via double resonance spectroscopy," *Appl. Phys. Lett.* **77**, 857 (2000).
doi:10.1063/1.1306651

[113] A. M. Alcalde and G. Weber, "Nonparabolicity effects on electron–optical-phonon scattering rates in quantum wells," *Phys. Rev. B* **56**, 9619 (1997).
doi:10.1103/PhysRevB.56.9619

[114] B. K. Ridley, *Quantum Processes in Semiconductors* Oxford Univ. Press 4th edn. (1999).
ISBN 0-19-850-580-9

[115] S. Sinning, T. Dekorsy, M. Helm, G. Mussler, L. Däweritz, and K. H. Ploog, "Reduced subpicosecond electron relaxation in GaN_xAs_{1-x}," *Appl. Phys. Lett.* **86**, 161912 (2005).
doi:10.1063/1.1904709

[116] U. Bockelmann and G. Bastard, "Phonon scattering and energy relaxation in two-, one-, and zero-dimensional electron gases," *Phys. Rev. B* **42**, 8947 (1990).
doi:10.1103/PhysRevB.42.8947

[117] V. Gorfinkel, S. Luryi, and B. Gelmont, "Theory of gain spectra for quantum cascade lasers and temperature dependence of their characteristics at low and moderate carrier concentrations," *IEEE J. Quantum Electron.* **32**, 1995 (1996).
doi:10.1109/3.541687

[118] C. Gmachl, F. Capasso, D. L. Sivco, and A. Y. Cho, "Recent progress in quantum cascade lasers and applications," *Rep. Prog. Phys.* **64**, 1533 (2001).
doi:10.1088/0034-4885/64/11/204

[119] J. Faist, "Quantum Cascade Lasers," in "Intersubband Transitions in Quantum Wells: Physics and Device Applications II," (edited by H. C. Liu and F. Capasso) vol. 66 of *Semiconductors and Semimetals* Academic Press (2000).
ISBN 0127521755

[120] Z. Liu, C. Gmachl, L. Cheng, F.-S. Choa, F. Towner, X. Wang, and J. Fan, "Temperature Dependence of Optical Gain and Loss in $\lambda \approx 8.2$–$10.2\,\mu$m Quantum-Cascade Lasers," *IEEE J. Quantum Electron.* **44**, 485 (2008).
doi:10.1109/JQE.2008.917273

[121] S. Rudin and T. L. Reinecke, "Electron–LO-phonon scattering rates in semiconductor quantum wells," *Phys. Rev. B* **41**, 7713 (1990).
doi:10.1103/PhysRevB.41.7713

[122] L. J. Olafsen, I. Vurgaftman, and J. R. Meyer, "Antimonide Mid-IR Lasers," in "Long-wavelength Infared Semiconductor Lasers," (edited by H. K. Choi) Wiley (2004). ISBN 0471392006

[123] V. Shastin, "Hot hole inter-sub-band transition p-Ge FIR laser," *Opt. Quantum Electron.* **23**, S111 (1991). doi:10.1007/BF00619761

[124] E. Bründermann, "Widely Tunable Far-Infared Hot-Hole Semiconductor Lasers," in "Long-wavelength Infared Semiconductor Lasers," (edited by H. K. Choi) Wiley (2004). ISBN 0471392006

[125] W. E. Pinson and R. Bray, "Experimental Determination of the Energy Distribution Functions and Analysis of the Energy-Loss Mechanisms of Hot Carriers in p-Type Germanium," *Phys. Rev.* **136**, A1449 (1964). doi:10.1103/PhysRev.136.A1449

[126] A. Wittmann, T. Gresch, E. Gini, L. Hvozdara, N. Hoyler, M. Giovannini, and J. Faist, "High-Performance Bound-to-Continuum Quantum-Cascade Lasers for Broad-Gain Applications," *Quantum Electronics, IEEE Journal of* **44**, 36 (2008). doi:10.1109/JQE.2007.909516

[127] Y. Yao, Z. Liu, A. J. Hoffman, K. J. Franz, and C. F. Gmachl, "Voltage Tunability of Quantum Cascade Lasers," *IEEE J. Quantum Electron.* **45** (2009).

[128] G. Wysocki, R. Lewicki, R. F. Curl, F. K. Tittel, L. Diehl, F. Capasso, M. Troccoli, G. Hofler, D. Bour, S. Corzine, R. Maulini, M. Giovannini, and J. Faist, "Widely tunable mode-hop free external cavity quantum cascade lasers for high resolution spectroscopy and chemical sensing," *Appl. Phys. B* **92**, 305 (2008). doi:10.1007/s00340-008-3047-x

[129] B. G. Lee, M. A. Belkin, R. Audet, J. MacArthur, L. Diehl, C. Pflügl, F. Capasso, D. C. Oakley, D. Chapman, A. Napoleone, D. Bour, S. Corzine, G. Höfler, and J. Faist, "Widely tunable single-mode quantum cascade laser source for mid-infrared spectroscopy," *Appl. Phys. Lett.* **91**, 231101 (2007). doi:10.1063/1.2816909

[130] M. Yamanishi, K. Fujita, T. Edamura, and H. Kan, "Indirect pump scheme for quantum cascade lasers: dynamics of electron-transport and very high T_0-values," *Opt. Express* **16**, 20748 (2008).
doi:10.1364/OE.16.020748

[131] J. Faist, F. Capasso, C. Sirtori, D. Sivco, A. Hutchinson, and A. Cho, "Laser action by tuning the oscillator strength," *Nature* **387**, 777 (1997).

[132] J. Faist, F. Capasso, C. Sirtori, D. L. Sivco, A. L. Hutchinson, and A. Y. Cho, "Vertical transition quantum cascade laser with Bragg confined excited state," *Appl. Phys. Lett.* **66**, 538 (1995).
doi:10.1063/1.114005

[133] C. Sirtori, J. Faist, F. Capasso, D. L. Sivco, A. L. Hutchinson, S. N. G. Chu, and A. Y. Cho, "Continuous wave operation of midinfrared (7.4–8.6 μm) quantum cascade lasers up to 110 K temperature," *Appl. Phys. Lett.* **68**, 1745 (1996).
doi:10.1063/1.116654

[134] C. Sirtori, F. Capasso, J. Faist, A. Hutchinson, D. Sivco, and A. Cho, "Resonant tunneling in quantum cascade lasers," *IEEE J. Quantum Electron.* **34**, 1722 (1998).
doi:10.1109/3.709589

[135] J. Faist, F. Capasso, C. Sirtori, D. L. Sivco, J. N. Baillargeon, A. L. Hutchinson, S. G. Chu, and A. Y. Cho, "High power mid-infrared ($\lambda \sim 5$ μm) quantum cascade lasers operating above room temperature," *Appl. Phys. Lett.* **68**, 3680 (1996).
doi:10.1063/1.115741

[136] C. Gmachl, A. Tredicucci, F. Capasso, A. L. Hutchinson, D. L. Sivco, J. N. Baillargeon, and A. Y. Cho, "High-power $\lambda \sim 8$ μm quantum cascade lasers with near optimum performance," *Appl. Phys. Lett.* **72**, 3130 (1998).
doi:10.1063/1.121569

[137] D. Hofstetter, M. Beck, T. Aellen, and J. Faist, "High-temperature operation of distributed feedback quantum-cascade lasers at 5.3 μm," *Appl. Phys. Lett.* **78**, 396 (2001).
doi:10.1063/1.1340865

[138] A. Lyakh, C. Pflügl, L. Diehl, Q. Wang, F. Capasso, X. Wang, J.-Y. Fan, T. Tanbun-Ek, A. Tsekoun, R. Maulini, R. Go, and C. K. N. Patel, "1.3 W quantum cascade lasers with optimized design for continuous-wave operation at room temperature," *Proc. Conference on Lasers and Electro-Optics* CTuF3 (2008).
url: http://ieeexplore.ieee.org/xpls/abs_all.jsp?arnumber=4571883

[139] M. C. Wanke, F. Capasso, C. Gmachl, A. Tredicucci, D. L. Sivco, A. L. Hutchinson, S.-N. G. Chu, and A. Y. Cho, "Injectorless quantum-cascade lasers," *Appl. Phys. Lett.* **78**, 3950 (2001).
doi:10.1063/1.1378805

[140] S. Katz, A. Friedrich, G. Boehm, and M.-C. Amann, "Continuous wave operation of injectorless quantum cascade lasers at low temperatures," *Appl. Phys. Lett.* **92**, 181103 (2008).
doi:10.1063/1.2841704

[141] H. Luo, S. R. Laframboise, Z. R. Wasilewski, G. C. Aers, H. C. Liu, and J. C. Cao, "Terahertz quantum-cascade lasers based on a three-well active module," *Appl. Phys. Lett.* **90**, 041112 (2007).
doi:10.1063/1.2437071

[142] M. A. Belkin, J. A. Fan, S. Hormoz, F. Capasso, S. P. Khanna, M. Lachab, A. G. Davies, and E. H. Linfield, "Terahertz quantum cascade lasers with copper metal-metal waveguides operating up to 178 K," *Opt. Express* **16**, 3242 (2008).
doi:10.1364/OE.16.003242

[143] R. Köhler, A. Tredicucci, F. Beltram, H. E. Beere, E. H. Linfield, A. G. Davies, D. A. Ritchie, R. C. Iotti, and F. Rossi, "Terahertz semiconductor-heterostructure laser," *Nature* **417**, 156 (2002).

[144] A. Evans, J. S. Yu, S. Slivken, and M. Razeghi, "Continuous-wave operation of $\lambda \sim 4.8$ µm quantum–cascade lasers at room temperature," *Appl. Phys. Lett.* **85**, 2166 (2004).
doi:10.1063/1.1793340

[145] A. Lyakh, C. Pflügl, L. Diehl, Q. J. Wang, F. Capasso, X. J. Wang, J. Y. Fan, T. Tanbun-Ek, R. Maulini, A. Tsekoun, R. Go, and C. K. N. Patel, "1.6 W high wall plug efficiency, continuous-wave room temperature quantum cascade laser emitting at 4.6 μm," *Appl. Phys. Lett.* **92**, 111110 (2008).
doi:10.1063/1.2899630

[146] K. Leo, *High-Field Transport in Semiconductor Superlattices* Springer, Berlin (2003).
ISBN 3-540-00569-2

[147] C. Gmachl, F. Capasso, A. Tredicucci, D. L. Sivco, R. Köhler, A. L. Hutchinson, and A. Y. Cho, "Dependence of the device performance on the number of stages in quantum-cascade lasers," *IEEE J. Sel. Top. Quantum Electron.* **5**, 808 (1999).
doi:10.1109/2944.788453

[148] P. G. Savvidis, B. Kolasa, G. Lee, and S. J. Allen, "Resonant Crossover of Terahertz Loss to the Gain of a Bloch Oscillating InAs/AlSb Superlattice," *Phys. Rev. Lett.* **92**, 196802 (2004).
doi:10.1103/PhysRevLett.92.196802

[149] J. B. Khurgin, Y. Dikmelik, P. Q. Liu, A. J. Hoffman, M. D. Escarra, K. J. Franz, and C. F. Gmachl, "Role of interface roughness in the transport and lasing characteristics of quantum-cascade lasers," *Appl. Phys. Lett.* **94**, 091101 (2009).
doi:10.1063/1.3093819

[150] E. Yablonovitch and E. Kane, "Band structure engineering of semiconductor lasers for optical communications," *J. Lightwave Technol.* **6**, 1292 (1988).
doi:10.1109/50.4133

[151] R. Dingle, W. Wiegmann, and C. H. Henry, "Quantum States of Confined Carriers in Very Thin $Al_xGa_{1-x}As$–GaAs–$Al_xGa_{1-x}As$ Heterostructures," *Phys. Rev. Lett.* **33**, 827 (1974).
doi:10.1103/PhysRevLett.33.827

[152] J. P. van der Ziel, R. Dingle, R. C. Miller, W. Wiegmann, and J. W. A. Nordland, "Laser oscillation from quantum states in very thin GaAs–$Al_{0.2}Ga_{0.8}As$ multilayer

structures," *Appl. Phys. Lett.* **26**, 463 (1975).
doi:10.1063/1.88211

[153] K. Choquette, K. Geib, C. Ashby, R. Twesten, O. Blum, H. Hou, D. Follstaedt, B. Hammons, D. Mathes, and R. Hull, "Advances in selective wet oxidation of AlGaAs alloys," *IEEE J. Sel. Top. Quantum Electron.* **3**, 916 (1997).
doi:10.1109/2944.640645

[154] C. Gmachl, F. Capasso, J. Faist, A. L. Hutchinson, A. Tredicucci, D. L. Sivco, J. N. Baillargeon, S. N. G. Chu, and A. Y. Cho, "Continuous-wave and high-power pulsed operation of index-coupled distributed feedback quantum cascade laser at $\lambda \approx 8.5$ µm," *Appl. Phys. Lett.* **72**, 1430 (1998).
doi:10.1063/1.120585

[155] L. Hvozdara, A. Lugstein, N. Finger, S. Gianordoli, W. Schrenk, K. Unterrainer, E. Bertagnolli, G. Strasser, and E. Gornik, "Quantum cascade lasers with monolithic air–semiconductor Bragg reflectors," *Appl. Phys. Lett.* **77**, 1241 (2000).
doi:10.1063/1.1289910

[156] S. Blaser, A. Bachle, S. Jochum, L. Hvozdara, G. Vandeputte, S. Brunner, S. Hansmann, A. Muller, and J. Faist, "Low-consumption (below 2W) continuous-wave singlemode quantum-cascade lasers grown by metal-organic vapour-phase epitaxy," *Electron. Lett.* **43**, 1201 (2007).
doi:10.1049/el:20072576

[157] Z. Liu, C. F. Gmachl, C. G. Caneau, and C. Zah, "Very Small ($\leq$ 1.2–1.7 W) Heat Dissipation, Room Temperature, Continuous-Wave Quantum Cascade Lasers at $\lambda \sim 5.3$ µm," *Proc. Conference on Lasers and Electro-Optics* CTuF2 (2008).
url: http://ieeexplore.ieee.org/xpls/abs_all.jsp?arnumber=4571882